Copy 6
RM E54L31

NACA

RESEARCH MEMORANDUM

EXPERIMENTAL INVESTIGATION OF A TRANSONIC COMPRESSOR

ROTOR WITH A 1.5-INCH CHORD LENGTH AND

AN ASPECT RATIO OF 3.0

I - DESIGN, OVER-ALL PERFORMANCE, AND

ROTATING-STALL CHARACTERISTICS

By Edward R. Tysl, Francis C. Schwenk, and Thomas B. Watkins

Lewis Flight Propulsion Laboratory
Cleveland, Ohio

NATIONAL ADVISORY COMMITTEE
FOR AERONAUTICS
WASHINGTON
March 28, 1955

3528

CY-1

NATIONAL ADVISORY COMMITTEE FOR AERONAUTICS

RESEARCH MEMORANDUM

EXPERIMENTAL INVESTIGATION OF A TRANSONIC COMPRESSOR ROTOR WITH A

1.5-INCH CHORD LENGTH AND AN ASPECT RATIO OF 3.0

I - DESIGN, OVER-ALL PERFORMANCE, AND ROTATING-STALL CHARACTERISTICS

By Edward R. Tysl, Francis C. Schwenk, and Thomas B. Watkins

SUMMARY

A transonic compressor rotor with double-circular-arc blade sections was designed and tested to investigate the aerodynamic effects of using a short blade chord and a high aspect ratio and to obtain more blade-element data. The design total-pressure ratio of this rotor was 1.35 at a corrected specific weight flow of 31.3 pounds per second per square foot frontal area with the rotor operating at a corrected tip speed of 1000 feet per second. The hub-tip radius ratio at the rotor inlet was 0.5. This report presents the rotor design, the over-all performance based on mass-averaged survey data behind the rotor, and the stall characteristics.

At design speed, a peak rotor efficiency of 0.91 was obtained at a corrected specific weight flow of 30 pounds per second per square foot frontal area with a mass-averaged total-pressure ratio of 1.32. At speeds lower than design, the peak efficiency was about 0.95. It was observed that the blade elements near the rotor tip had the greatest effect on the variations of mass-averaged efficiency with speed and weight flow.

Rotating stalls were observed at 50, 60, and 80 percent design speed in addition to a surge characteristic at 80 percent design speed. For this compressor rotor, one or two full-span rotating-stall zones were noted. Blade vibrations appeared to be greater for operation with two stall zones.

INTRODUCTION

One phase of the research on axial-flow compressors for aircraft tur-bomachinery has been directed toward reducing the size and weight of the compressors without compromising the efficiency level. For a given application, the size and weight of the compressor can be reduced by increasing

the flow capacity per unit of frontal area and by increasing the total-
pressure ratio per unit of compressor length. Consequently, it was of
primary importance to study stages of large flow capacity capable of
producing high pressure ratios.

The results of testing transonic axial-flow compressors (refs. 1 to
3) have shown that it is possible in one stage to produce high total-
pressure ratios at high mass flows with no decrease in efficiency over
conventional subsonic stages. References 4 and 5 have demonstrated the
feasibility of using high-pressure-ratio transonic stages in multistage
compressors in which the number of stages required to produce a given
over-all compressor pressure ratio has been reduced in comparison with
the number of stages used in subsonic compressors. Since most of the
research transonic compressors tested have been constructed with long-
chord low-aspect-ratio blading, transonic compressors with high pressure
ratios and high flow capacities will be more useful if their chord lengths
can be reduced without affecting the efficiency levels.

A reduction of the chord length of a transonic compressor rotor be-
low the values for which there is some experience involves both structur-
al and aerodynamic considerations. In this report, the aerodynamic ef-
fects of the use of a short chord length in a transonic compressor rotor
are considered. Chord length will influence to some extent the losses
(efficiency), the applicability of a simplified-radial-equilibrium equa-
tion to design and analysis, and the control of the blade shape in fabri-
cation. A change in chord length will affect the losses through a change
in the blade-chord Reynolds number, the velocity gradients on the surfaces
of the blade elements, and the three-dimensional effects (secondary flows
and blade-end effects). The streamline curvature should increase with a
reduction in chord length (increased aspect ratio) and thereby may become
an important factor in the radial-equilibrium equation. Fabrication
control of blade angles and thickness, which is more difficult with small
chord lengths, may be important with respect to the performance of high
Mach number, high-pressure-ratio compressor rotors.

Although all these aerodynamic effects may exist, it is not known
whether they are important. Therefore, an exploratory investigation of
a 1.5-inch-chord transonic rotor was initiated at the NACA Lewis labora-
tory to study the aerodynamic effects of a reduction in chord length
below current values.

The 1.5-inch-chord transonic axial-flow compressor rotor was designed
for application in the inlet stage of multistage compressors of current
interest. The rotor-inlet relative Mach number at the tip and the rotor-
tip diffusion factor were set at values that have previously been em-
ployed; a design corrected tip speed of 1000 feet per second was selected.
For these specifications and for a rotor-inlet hub-tip radius ratio of
0.5, the design corrected specific weight flow is 31.3 pounds per second

per square foot of frontal area, and the design rotor total-pressure ratio
is approximately 1.35. The aspect ratio of the rotor blade (based on the
inlet blade height) is 3.0 for an 18-inch rotor-tip diameter. Double-
circular-arc airfoils were chosen for the blade sections.

This report presents the rotor design procedure, which includes an
estimation of the radial variation of blade-element losses. Preliminary
information regarding the aerodynamic characteristics of the 1.5-inch-
chord transonic compressor rotor is presented as the mass-averaged over-
all performance and radial variations of rotor-inlet and -outlet flow
conditions. Since rotating stalls can cause blade-vibration problems,
these characteristics were investigated with hot-wire anemometers and
are presented herein. Blade vibrations were qualitatively observed with
the aid of a magnetic vibration pickup.

COMPRESSOR DESIGN

General Considerations

A transonic compressor rotor of short chord length and high aspect
ratio was designed for application in an inlet stage of current multi-
stage, axial-flow compressors. The basic design assumption made was that
the design procedure derived from past experience with long-chord tran-
sonic compressor rotors would be applicable to the design of a transonic
compressor rotor of short chord length. Specifically, it was assumed that
the simplified-radial-equilibrium concept would adequately predict the
radial distribution of the rotor-outlet flow conditions, that the blade-
element approach to blade selection would be correct, and that the
diffusion-factor analysis of reference 6 would apply to the estimation
of the blade-element losses.

The design characteristics (or velocity diagrams) were selected to
be in the range of conditions for which high-efficiency operation had
been experienced in the past. The design calculations considered a radial
variation in the relative total-pressure-loss coefficient $\bar{\omega}$ and the
aerodynamic characteristics of an axial-discharge stator row. The rotor
was designed for a radially constant total-pressure ratio.

The design velocity diagrams were computed along stream surfaces
generated by rotating assumed streamlines in the rz-plane about the rotor
axis. For simplicity, the streamlines that lie in the rz-plane were
assumed to be straight lines which divide the annulus height into equal-
percentage radial increments at the inlet and outlet of the blade row.
Seven streamlines were used to describe the design flow conditions.

On the basis of past experience with transonic compressor rotors,
the rotor tip solidity (chord spacing ratio) was set approximately equal
to 1.0 (final rotor-tip solidity equaled 0.95).

3528

CY-1 back

Design Rotor-Inlet Conditions and Weight Flow

A moderate corrected tip speed of 1000 feet per second was selected, because it was then possible to obtain a relatively high total-pressure ratio and high specific weight flow for relative inlet Mach numbers in the range of values which have been used previously. For the purposes of this investigation, the design value of rotor-inlet relative Mach number was set at 1.15 at the tip. (This value should not be construed as a limiting Mach number.) It was decided that no guide vanes should be used (axial inlet velocity), and the inlet hub-tip radius ratio was taken as 0.5.

Results of a test program conducted in the same research facility as was used for this investigation revealed the presence of a radial variation of inlet absolute Mach number for zero prewhirl. This radial gradient, shown in reference 7, was utilized in specifying the design inlet conditions for the 1.5-inch-chord transonic compressor rotor. The test results reported in reference 7 also provide a value of 0.985 for the wall-boundary-layer blockage factor at the rotor inlet.

The preceding conditions fixed the design corrected specific weight flow at 31.3 pounds per second per square foot of frontal area. The calculated absolute inlet Mach number was 0.62 at the mean radius, which corresponds to a velocity of 666.5 feet per second at NACA standard conditions.

Annulus-Area Variation and Preliminary Velocity-Diagram Calculation

Before proceeding with the calculation of the design velocity diagrams, the annulus-area variation or hub contour for a constant-tip-diameter stage was established. By estimating the stage (rotor plus stator) total-pressure ratio and efficiency, the stator-outlet hub radius (5.19 in.) was calculated for an axial discharge velocity of 600 feet per second. From an assumption of the axial depth of the stage, a curve was faired between the existing inlet hub section and the stator-outlet station. Downstream of the stators a constant hub radius was maintained. Since the fairing process was somewhat arbitrary, the hub-contour curve served only as a guide in the selection of a rotor-outlet hub radius that would provide desirable rotor and stator blade-element loadings (diffusion factors). A preliminary calculation of the design velocity diagrams determined the desirable value for the rotor-outlet hub radius and the approximate rotor total pressure for a tip diffusion factor of 0.4. An assumption of radially constant efficiency facilitated the calculation. (Ref. 2 gives an example of this type of velocity-diagram calculation.) The efficiency was arbitrarily set at 0.96, a reasonable value for the flow outside the wall-boundary-layer regions. As a result of the preliminary design, the rotor-outlet hub radius was set at 5.00 inches at a

proposed measuring station about 1/2-inch downstream of the rotor disk. It was also indicated that a rotor total-pressure ratio of about 1.37 could be obtained for a tip diffusion factor of 0.4.

Final Velocity-Diagram Calculations

The results of the preliminary calculation served as the starting point for the more detailed design procedure, which includes the radial variations of the rotor losses. A constant rotor total-pressure ratio was maintained.

Blade-element losses $\left(\bar{\omega} = \dfrac{(P'_4)_i - P'_4}{P'_3 - p_3}\right)$ for the hub, mean, and tip

sections of the rotor were selected from the data of reference 6 and were based on values of diffusion factor computed in the constant-loss solution. By plotting these losses against radius (fig. 2), the blade-element losses for other sections were determined.

With the design values of blade-element losses given, the radial variation of total-temperature ratio can be computed by the following equations, which are derived in reference 6. (All symbols are defined in appendix A, and a typical velocity diagram is shown in fig. 1.) The blade-element recovery factor R.F. can be written as

$$R.F. = 1 - \frac{\bar{\omega}}{\left(\dfrac{P'_4}{P'_3}\right)_i} \left[1 - \left(\cfrac{1}{1 + \dfrac{\gamma-1}{2} M'^2_3}\right)^{\frac{\gamma}{\gamma-1}}\right] = \frac{P'_4}{P'_3}\bigg/\left(\frac{P'_4}{P'_3}\right)_i$$

in which all quantities refer to a streamline or a blade element. The ideal relative total-pressure ratio $(P'_4/P'_3)_i$ is created by the radius change of the streamline and is

$$\left(\frac{P'_4}{P'_3}\right)_i = \left\{1 + \frac{\gamma-1}{2} \frac{U^2_4}{a'^2_{0,3}} \left[1 - \left(\frac{r_3}{r_4}\right)^2\right]\right\}^{\frac{\gamma}{\gamma-1}}$$

From the definition of recovery factor,

$$\frac{T_4}{T_3} = \left(\frac{\dfrac{P_4}{P_3}}{R.F.}\right)^{\frac{\gamma-1}{\gamma}}$$

Thus, the total state for each radial position downstream of the rotor can be determined.

The rotor-outlet tangential velocity is given by

$$V_{\theta,4} = \frac{a_{0,3}^2}{2\pi N r_4 (\gamma - 1)} \left(\frac{T_4}{T_3} - 1\right)$$

The static conditions (or velocities) must satisfy the prescribed simplified-radial-equilibrium equation $\left(\dfrac{dp}{dr} = \dfrac{\rho}{g}\dfrac{V_\theta^2}{r}\right)$, which mainly predicts a gradient, and the continuity equation, which establishes the level of the static conditions.

The following calculation procedure indicates one of perhaps many methods available to determine the static state (or velocities). By integrating the simplified-radial-equilibrium equation, the following equation results:

$$P_{4,t} - P_4 = \int_{r_4}^{r_{4,t}} \frac{\rho_4 V_{\theta,4}^2}{g r_4}\, dr_4 \qquad (1)$$

The values of static density ρ_4 and static pressure p_4 are both unknown and are interdependent. Consequently, the solution of equation (1) requires an iteration process.

The calculation of the static pressures by equation (1) started with the assumption of a static-pressure variation, based upon the results of the preliminary constant-loss design study. Static densities ρ_4 were were computed from

$$\frac{\rho_4}{\rho_{0,4}} = \left(\frac{p_4}{P_4}\right)^{1/\gamma}$$

3528

By means of a step-by-step numerical integration of the right side of equation (1), a new static-pressure variation was determined with the general level of the results established by the value of the assumed static pressure at the tip or outer wall $p_{4,t}$. The computed static-pressure variation was then used as a second trial, and the process repeated. Fortunately, the solution of equation (1) converges very rapidly to correct values of static pressure; therefore, generally, no more than two iterations should be required to determine the simplified-radial-equilibrium static-pressure distribution accurately.

The level of the rotor-outlet static pressures p_4 must satisfy the continuity concept

$$W_3 = W_4 = 2\pi K_4 \int_{r_{h,4}}^{r_{t,4}} \rho_4 V_{z,4} r_4 dr_4$$

where the boundary-layer blockage factor K_4 (defined in ref. 5) was assumed to be 0.96, a value taken from transonic single-stage compressor test results. The axial velocity $V_{z,4}$ was defined as

$$V_{z,4} = \sqrt{V_4^2 - V_{\theta,4}^2}$$

Inherent in this definition for axial velocity is the assumption that the radial component of the velocity is negligible. The outlet weight flow was computed for the static pressures given by equation (1), and the level of the rotor-outlet static pressures was adjusted until the rotor-outlet weight flow W_4 equaled the inlet weight flow W_3. In this process, the variation of static pressure was maintained parallel to the static-pressure distribution given by equation (1). Finally, the static-pressure variation that satisfied continuity was checked against simplified radial equilibrium (eq. (1)), since the level of static pressure will affect the gradient to some extent. The resulting static pressures, which satisfied both equilibrium and continuity, permitted the calculation of the rotor-outlet vector-diagram components.

The variable-loss design calculations gave a variation of rotor-outlet axial velocity with radius; the axial velocity at the tip was lower than that at the hub. As a consequence, the resulting rotor-tip diffusion factor D was about 0.42 for a total-pressure ratio of 1.37, compared with the diffusion factor of 0.40 for the constant-efficiency design at the same total-pressure-ratio level. In order to reduce the rotor-tip diffusion factor to a value of 0.40, the design total-pressure ratio was set at 1.35 (radially constant), and the velocity diagrams were recomputed according to the preceding method. The design data for a total-pressure ratio of 1.35 are given in table I.

The design total-pressure ratio of 1.35 represents a free-stream value and is somewhat higher than the expected average total pressure, which would include the deficiency of total pressure in the wall boundary layers. A free-stream mass-averaged efficiency was computed to be 0.93; again, an average rotor efficiency that includes wall-boundary-layer effects should be several points lower than this value.

Blade Selection

A compressor blade is designed by radially stacking blade elements or sections which are selected to produce the desired aerodynamic performance. Double-circular-arc airfoils were chosen as the blade sections. The complete specification of the blade sections required assumptions of incidence and deviation angles and blade thickness, which depend, in part, on the solidity of the blade row. Therefore, determination of the chord length, tip diameter, and the number of blades was established as the first step in the blade selection.

Blade solidity. - A chord length of 1.5 inches, constant over the blade span, was chosen - a value representative of chord lengths utilized in subsonic, multistage, axial-flow compressors. High-aspect-ratio blades (long span and short chord) were also desired, but the span of the blades was limited by the air-flow capacity of the test facility. For an inlet hub-tip radius ratio of 0.5, the air-flow capacity fixed the tip diameter at 18 inches. The number of blades was set at 35 to provide a solidity of about 1.0 at the rotor tip. The aspect ratio for this configuration is 3.0 based on the blade span at the inlet of the rotor.

Design incidence and deviation angles. - Design incidence angles (assumed to be the minimum-loss incidence angle) were estimated with the aid of available rotor-blade-element data. The design incidence angle was set at 3° at the tip and 6° at the hub and varied linearly over the blade span.

Incompressible, potential-flow theory requires negative design incidence angles for cascades having the high camber of a rotor hub section; however, rotor test data show that minimum-loss operation occurs at positive incidence angles. Analysis of the channel area variation (along the flow path) for blade sections near the hub of rotors reveals that the incidence angle must be positive in order to avoid choking with operation at high subsonic values of inlet relative Mach number. On this basis, the high hub-section design incidence angles are reasonable.

Deviation angles were computed from Carter's rule (ref. 8). Examination of available blade-element data for double-circular-arc airfoils in annular cascades (rotors and stators) (e.g., refs. 7 and 9) indicated that Carter's rule was a reasonable design approach for rotor blade

3528

CU-2

sections between the tip and mean regions. For the sections near the hub, the design values of deviation angle were arbitrarily increased about 1° to 2° over the values computed from Carter's rule. The design values of incidence and deviation angles are given in table I.

Blade thickness. - At the tip of the rotor, the maximum blade thickness was set at 6 percent of the chord length as a result of previous experience with transonic compressor rotors. The maximum thickness for the blade element along the hub stream surface (blade root) was set at about 10 percent of the chord length. The choice of hub-section thickness was based on structural considerations and calculations of the channel areas between two adjacent blade elements. The maximum thickness was varied hyperbolically along the blade span because of stress requirements.

For each blade element, the leading-edge radius equaled the trailing-edge radius. The radii at the tip section were set at 0.010 inch, which should allow good performance at high Mach numbers and cause no fabrication difficulties. To ease blade-root stresses, large leading- and trailing-edge radii for the hub section are required; however, a limit is reached when channel areas and choking are considered. As a consequence, the radii for the hub section were set at 0.020 inch. Leading- and trailing-edge radii were varied linearly over the blade span.

Specification of blade sections for fabrication purposes. - Since the design performance was computed for flow along conical stream surfaces, the blade sections were considered to lie on the stream surfaces. For fabrication of the rotor blades, it was necessary to provide section coordinates for constant-radius cross sections of the blade (sections that lie on a cylindrical surface). One procedure for providing such blade coordinates entails a graphical interpolation of the blade-section coordinates that lie on the conical stream surfaces.

In the case of this design a somewhat simpler method was used to specify the blade for fabrication. The desired inlet and outlet mean-camber-line angles of the blade sections on conical surfaces (as determined from the design relative air directions and incidence and deviation angles) were converted to mean-camber-line angles of blade sections on cylindrical surfaces according to equation (B6) (appendix B). Double-circular-arc airfoil coordinates were then calculated for the blade-inlet and -outlet mean-camber-line angles on the cylindrical surfaces, and the rotor blade was fabricated from these blade sections.

With this procedure blades can be produced that have the desired blades angles for sections on the assumed stream surfaces; however, the blade elements will not generally be the desired shape (double-circular-arc airfoils in this case). In most cases, the differences between the actual blade shape and the desired blade shape (as regards the camber-line shape and thickness distribution) will be small.

The blade mean-camber-line angles were measured from a completed
blade for cross sections approximating the sections of the blade that lie
on stream surfaces of revolution. The results of this measurement as well
as the design blade angles are shown in figure 3. Analysis of the blade-
row performance is based on the measured blade angles.

APPARATUS AND PROCEDURE

Compressor Installation

The short-chord transonic compressor rotor was installed in a
variable-component test rig. Figure 4 shows a sketch of this installa-
tion, and figure 5 is a photograph of the compressor rotor. A 3000-
horsepower variable-frequency motor in conjunction with a speed-increasing
gearbox supplied power to this compressor rotor. Tests conducted on
the rotor used atmospheric air drawn through a thin-plate sharp-edged
orifice into a depression tank. The air entered the test compressor from
the depression tank through a bellmouth. The compressor discharged the
air into an annular passage, which connected to a radial diffuser that
led to the laboratory exhaust system.

Instrumentation

A thin-plate sharp-edged orifice was used to measure the air flow
through the compressor. Pressure drop across the orifice was indicated
on a micromanometer. Orifice temperature was measured by two iron-
constantan thermocouples.

The location of the instrumentation in the test rig is shown in
figure 4. Station 1 is located in the depression tank (4 ft in diam.
and approximately 6 ft long) ahead of the test section and is not shown
in figure 4. Stations 2 and 3 are 1.52 and 0.33 inches upstream of the
rotor disk, respectively. Station 4 is located 0.51 inch downstream of
the rotor.

Inlet stagnation conditions were determined from six total-pressure
probes and six total-temperature probes located at centers of equal annu-
lar areas in the depression tank. At station 2, a five-tube radial L
static-pressure probe (fig. 6(a)) measured the static-pressure variation
across the annulus in conjunction with four outer-wall and four inner-wall
static-pressure taps spaced approximately equally around the circumference.
The instrumentation at station 3 consisted of four outer-wall and four
inner-wall static-pressure taps equally spaced around the circumference.

Rotor-outlet conditions were obtained by radial surveys of static
and total pressure, total temperature, and flow angle at station 4. These

surveys were made by the two types of instruments shown in figure 6(b) and (c). Three combination probes were spaced circumferentially and were used to measure flow angle, total pressure, and total temperature. Each probe obtained data at 11 radial positions across the 4-inch passage. Static pressures were obtained by two circumferentially spaced wedge static probes. Each wedge static probe measured static pressures at only six of the 11 radial positions mentioned previously. The distance from either wall to the first static-pressure survey station was equal to 16 percent of the passage height. Data from survey probes were averaged at each radial position, and then the static pressures and total temperatures were corrected for local Mach number effects.

The flow fluctuations of rotating stall were detected with constant-temperature hot-wire anemometers. The anemometer probes were made with 0.0002-inch-diameter tungsten wire with an effective length of 0.08 inch. Observations were made with a dual-beam oscilloscope. The auxiliary equipment used is that discussed in reference 10. Two hot-wire-anemometer probes were installed in radially traversing mechanisms about 1/2 inch downstream of the rotor (station 4). Three survey locations on the circumference were used to vary the angle between the two probes to permit the determination of the number of stall zones (ref. 11).

Over-All Performance Tests

The rotor was operated over a range of weight flow at corrected tip speeds of 600, 700, 800, 900, and 1000 feet per second. Maximum weight flow was limited by pressure ratio at the lower speeds and rotor or system choking at the higher speeds. Minimum weight flow investigated at all speeds was limited by blade vibrations. The vibrations were detected on an oscilloscope which was connected to a magnetic-type vibration pickup mounted on the casing a small distance upstream of the leading edge of the compressor.

The depression-tank pressure was maintained constant at 20 inches of mercury absolute. Depression-tank temperatures varied from 65° to 85° F, depending on the ambient temperature of the test cell. The blade-chord Reynolds number at design speed and at the tip of the rotor was approximately 500,000.

Over-all rotor performance was obtained by mass averaging the blade-element performance at station 4 as outlined in reference 7.

Rotating-Stall Characteristics

After rotor performance data had been obtained, hot-wire anemometers were used to investigate the stall patterns behind the rotor for 50, 60, and 80 percent of design speed. The number of rotating-stall regions was determined by the methods described in reference 11.

RESULTS AND DISCUSSION

Over-All Performance

The over-all performance of the 1.5-inch-chord transonic compressor rotor is shown in figure 7. Mass-averaged total-pressure ratio and mass-averaged adiabatic temperature-rise efficiency are plotted against equivalent weight flow per unit frontal area $W\sqrt{\theta}/\delta A_f$ for corrected tip speeds of 100, 90, 80, 70, and 60 percent of design.

Weight flow. - At design speed, the rotor choked at design weight flow as indicated by the vertical performance line (fig. 7). The rotor might have been made to operate in an unchoked condition at design weight flow by selecting higher design incidence angles for the blade sections, thus increasing the blade passage area.

The weight-flow range investigated decreased as the Mach number (rotor speed) increased. For example, at a tip speed of 600 feet per second, the weight-flow range was approximately 11.3 pounds per second per square foot; while at design speed, the range had decreased to about 3.5 pounds per second per square foot (fig. 7). Further comparison of weight-flow range can be made from figure 8, where the mass-averaged work coefficient and a mass-averaged temperature-rise efficiency are plotted against a mean-radius flow coefficient $\varphi = (V_{z,3}/U_3)_m$. Figure 8 indicates that weight-flow range is restricted at both high and low values of flow coefficient φ as speed is increased. Figure 8 also indicates that the mass-averaged work coefficient $\Delta H/U_t^2$ is not constant with changes in speed. This compressibility effect, which is associated with high total-pressure ratios, has been observed with other high-pressure-ratio transonic compressor rotors (e.g., ref. 7).

Pressure ratio and efficiency. - The peak measured adiabatic efficiency at design speed was 0.91 with a corrected weight flow of 30 pounds per second per square foot and a total-pressure ratio of 1.32. The difference between the experimental values of mass-averaged efficiency and total-pressure ratio and the design values may be due in part to the losses encountered in the blade end regions. The design values, 0.93 for efficiency and 1.35 for total-pressure ratio, were calculated on the basis of blade elements without considering boundary-layer or wall effects.

The peak efficiency at speeds lower than design speed was approximately 0.95.

Rotor-Inlet Conditions

The computations of inlet conditions were made with the absolute inlet velocity considered axial in direction (no inlet guide vanes). The

static-pressure variation along the radius at the rotor inlet (station 3) was faired between the outer- and inner-wall static tap readings with a trend similar to that recorded from the inlet static-pressure rake (station 2). The procedure was considered justifiable, because there was only a small difference between the wall static pressures at stations 2 and 3.

To represent rotor-inlet (and rotor-outlet) conditions at 60, 80, and 100 percent design speed, three test points were selected at each speed. These test points represent high weight flow, maximum pressure ratio, and maximum-efficiency operation of the rotor.

Figure 9(a) shows the variation with radius of the ratio of inlet absolute Mach number to inlet absolute Mach number at mean radius $(M_3/M_{3,m})$. The design variation of inlet absolute Mach number was determined from previous tests using about the same inlet configuration. Comparison between measured and design values of inlet absolute Mach number was very good except at the low flow occurring at 60 percent design speed. This is probably an effect of radial redistribution of flow through the rotor due to stalling and poor flow conditions at the rotor tip.

Comparison of measured and design relative inlet Mach numbers can be made from figure 9(b). The radial slopes of the curves measured for values of relative inlet Mach number M'_3 compare very well at design speed, especially at maximum weight flow, although the values are different. The difference in level between design and measured values of relative inlet Mach number for peak-efficiency operation is reflected in the lower than design weight flow. As the speed is lowered, the inlet relative Mach number gradient is reduced.

Figure 9(c) shows the variation of rotor-inlet relative air angle β'_3 with radius. The design-air-angle variation and measured blade-inlet angle γ^o_3 (repeated from fig. 3) are also shown. At design speed, the variation of the rotor-inlet relative air angle that most nearly matches the design value is obtained at the choked-flow point - a further indication that the design values of incidence angles were too low to allow the passage of the design weight flow.

Rotor-Outlet Conditions

Figure 10 presents the rotor-outlet conditions as computed from the survey instrument measurements at station 4. The data shown are the radial variations of blade-element total-pressure ratio and temperature-rise efficiency, rotor-outlet Mach number, and rotor-outlet absolute flow direction for the same test points discussed in the section Rotor-Inlet

Conditions. The predicted design radial variations of rotor-outlet conditions are also given in figure 10(a) along with the experimental variations for operation of the rotor at design speed.

Efficiency. - The radial variations of efficiency show that the blade elements near the tip have the greatest effect on the variations of the mass-averaged efficiency with speed and weight flow. That is, consideration of the mass-averaged peak-efficiency operation point for each speed shown in figure 10 indicates that the blade-element efficiency near the hub and at the mean radius does not vary much with speed. On the other hand, the blade-element efficiency near the tip does vary with speed, as shown by comparison of the blade-element efficiencies for 80 and 100 percent of design speed. At a given speed, efficiency variations with weight flow are most apparent for the blade elements near the tip.

Over a large portion of the passage, the predicted design radial variation of blade-element efficiency agrees with measured variation for mass-averaged peak-efficiency operation at design speed.

Pressure ratio. - Figure 10 shows that the largest variation of total-pressure ratio with weight flow (at constant speed) occurs near the tip of the rotor. This characteristic has been observed previously (ref. 7) and can be explained on the basis of the velocity diagrams, as is done in reference 7.

At design speed, the measured total-pressure ratio is approximately constant over the major portion of the passage height for operation at the mass-averaged peak-efficiency point. The fall-off in total-pressure ratio near the inner and outer walls is probably caused by wall boundary layers and other end effects. The measured total-pressure-ratio level (at design speed and peak efficiency) is slightly lower than the design value of 1.35.

Rotor-outlet absolute flow angles and Mach numbers. - Compared with the variation of the design rotor-outlet flow angle, the measured results (fig. 10(a)) indicate a smaller radial variation in the central or free-stream portion of the passage (for peak-efficiency operation at design speed). Near the outer wall the measured angles increase rapidly from the free-stream values; this is an indication of wall-boundary-layer effects. At the lower speeds, there is a larger radial variation in rotor-outlet flow angle than at design speed.

The measured absolute Mach number variation (at design speed and peak efficiency, fig. 10(a)) agrees closely with the design variation, although the measured level is lower than the design level.

3528

The design of a set of stators for this rotor would not be too dif-
ficult. If the stators were designed to match the flow at peak efficiency
and design speed of the rotor, the inlet-stator Mach number would not ex-
ceed 0.7 and the inlet angle would be approximately 30°.

Rotating-Stall Characteristics and Blade Vibrations

Observations of rotating-stall characteristics were made with hot-
wire anemometers at several corrected tip speeds. Figure 11, a portion
of the mass-averaged over-all performance map (fig. 7), indicates the
operating ranges over which the various unsteady flow phenomena were ob-
served at 60 and 80 percent of design speed. The letters on figure 11
denote the beginning of a particular type of unsteady flow phenomenon for
decreasing weight flow.

Blade vibrations sensed by a magnetic vibration pickup were also
observed on an oscilloscope. The vibration information is only qualita-
tive, however, because an accurate calibration of the vibration pickup
was not possible.

At high weight flows at 60 and 80 percent of design speed, blade
wakes could be observed over the entire span except in small regions near
the inner and outer walls. Near the walls, air-flow fluctuations of a
random nature were detected. As peak-pressure-ratio operation was ap-
proached by decreasing the weight flow, the region of unsteady flow near
the rotor tip increased in extent until about 10 percent of the passage
was affected at the peak-pressure-ratio point on each speed curve
(fig. 11).

A further decrease in weight flow at 60 percent of design speed led
to a rotating-stall condition at point A (fig. 11). Two stall zones were
observed rotating in the direction of rotor rotation at an absolute speed
of 79 rps. The stall zones covered the entire blade span. The amplitudes
of the traces on the oscilloscope were constant for all radial positions
of the hot wires (except close to the walls). Blade vibrations were also
present, as indicated by the magnetic vibration pickup.

At point B (60 percent of design speed) a single, full-span rotating-
stall zone was observed. The absolute stall speed was 75 rps in the di-
rection of rotor rotation. The blades vibrated at this condition, but
the vibrations were not so great as those noted at point A.

For weight flows lower than that at point B at 60 percent of design
speed, the single stall zone was stable; that is, the type of stall, num-
ber of stall zones, and stall-zone speed did not alter. However, the
circumferential extent of the stall zone increased with decreasing weight
flow.

At point C (fig. 11, 80 percent of design speed), a flow fluctuation caused the two hot-wire anemometers to produce oscilloscope traces which were always in phase regardless of the circumferential spacing between the two probes. This phenomenon was an axial pulsation, or surge, and not a periodic rotating-stall condition. The frequency of the pulsation was 36 cps. The surge pulsations were greatest near the tip and had an amplitude of nearly zero at the mean and lower radii.

The characteristics of the surge phenomenon (frequency and operating condition at which it appears) depend on the volumes and resistances of the parts of the air-flow system. Therefore, if this rotor had been tested in a different research facility, the surge characteristics described probably would not have been duplicated. Furthermore, the surge characteristics of a complete turbojet engine (of which this compressor rotor may be a part) probably would not be the same as those reported.

At point D, a single, full-span rotating-stall zone was again observed. The absolute stall-zone speed was 96 rps in the direction of rotor rotation. Blade vibrations were present but not serious.

Rotating stalls were also investigated at 50 percent of design speed for decreasing weight flows. As at 60 percent of design speed, two full-span rotating-stall zones were first observed, and then a single stall-zone condition was noted. The rotational speeds of the stall zones were 65 and 60 rps, respectively, for the two conditions. The disturbances caused by the two rotating-stall zones produced greater blade vibrations than were observed during operation with the single stall zone.

Table II summarizes the rotating-stall characteristics. The values of h'/N (ratio of relative stall speed to rotor speed) are approximately constant for each stall condition (one or two stall zones). Another transonic rotor (ref. 2) exhibited operation with two full-span rotating-stall zones. As reported in reference 2, the value of h'/N was 0.37 at this condition, which agrees closely with the values given in table II for operation with two stall zones.

Since the blades vibrated more with two stall zones than with one stall zone, the frequency of the disturbances caused by the rotating-stall zones was compared with the natural frequency of the blades to determine whether a correlation can be made. The disturbance frequency is the product $\lambda h'$ of the relative rotational speed of the stall zones and the number of stall zones. Blade natural frequencies f were determined from a measurement of the natural frequency while the rotor was stationary from equations (188) and (189) of reference 12.

The disturbance frequencies and the blade natural frequencies are compared in table II by means of the ratio $\lambda h'/f$. It can be seen that

3528

the disturbance frequencies associated with two-stall operations at 60 and 50 percent of design speed are close to the second and third harmonics, respectively, of the blade natural frequency; at these two conditions, the largest blade vibrations were observed. For operation with one stall zone, the ratios of disturbance frequency to blade natural frequency are lower than with two stall zones; and the resulting blade vibrations were considerably smaller.

SUMMARY OF RESULTS

The following preliminary results were obtained from an experimental investigation of a short-chord transonic axial-flow compressor rotor with double-circular-arc airfoil blade sections. This rotor was designed and tested to investigate the aerodynamic effects of using short chords and high aspect ratios and to obtain more blade-element data. The rotor was designed for a radially constant total-pressure ratio of 1.35, with a design rotor-inlet relative Mach number at the tip of 1.15 at a corrected tip speed of 1000 feet per second and an inlet hub-tip ratio of 0.5.

1. The peak efficiency at design speed, as determined from mass-averaged survey data, was 0.91 at a corrected specific weight flow of 30 pounds per second per square foot frontal area and a mass-averaged total-pressure ratio of 1.32. At the lower speeds, the peak efficiency was approximately 0.95.

2. The data show that the blade elements near the rotor tip have the greatest effect on the variations of the mass-averaged efficiency with speed and weight flow.

3. For this rotor, full-span rotating stalls in either one or two stall zones were observed; surge at 80 percent of design speed was produced as the weight flow was decreased.

4. Blade vibrations were greater for operation with two stall zones than with one stall zone.

Lewis Flight Propulsion Laboratory
    National Advisory Committee for Aeronautics
        Cleveland, Ohio, December 28, 1954

APPENDIX A

SYMBOLS

The following symbols are used in this report: A diagram illustrating the air and blade angles and the velocities is presented in figure 1 to more completely define some of the symbols used.

A_f compressor frontal area based on rotor-tip diameter, 1.767 sq ft

a   velocity of sound, ft/sec

c_p specific heat of air at constant pressure, Btu/(lb)(^{O}R)

c_v specific heat of air at constant volume, Btu/(lb)(^{O}R)

g   acceleration due to gravity, 32.17 ft/sec^2

H   total enthalpy, $c_p g J T$, sq ft/sec^2

i   incidence angle, angle between inlet-relative-air-velocity vector and tangent to blade mean camber line at leading edge, deg

J   Joule's constant, 778.26 ft-lb/Btu

M   Mach number

N   rotor rotational speed, rps

P   total pressure, lb/sq ft

p   static pressure, lb/sq ft

r   radius measured from axis of rotation, in.

T   total temperature, ^{O}R

U   blade speed, ft/sec

V   air velocity, ft/sec

W   weight flow of air, lb/sec

z   axial direction

β   air-flow angle measured from axis of rotation, deg

3528

γ ratio of specific heats for air, c_p/c_v, 1.40

γ^o blade angle, direction of tangent to blade mean camber line at leading or trailing edge, deg

δ ratio of inlet total pressure to NACA standard total pressure, $P_1/2117$

δ^o deviation angle, angle between outlet-relative-air-velocity vector and tangent to blade mean-camber-line angle at trailing edge, deg

η temperature-rise efficiency

θ ratio of compressor-inlet total temperature to NACA standard temperature, $T_1/518.6$

ρ static density of air, lb/cu ft

φ rotor-inlet flow coefficient at mean radius, $\left(\dfrac{V_{z,3}}{U_3}\right)_m$

$\bar{\omega}$ relative total-pressure-loss coefficient (ref. 7)

Subscripts:

h   hub

i   ideal

m   mean radius

t   tip of rotor

z   axial direction

θ tangential direction

0   total or stagnation conditions

1   depression tank

2   upstream of rotor, location of inlet static-pressure rake

3   rotor inlet

4   rotor-outlet survey station

Superscript:

'   denotes conditions relative to blade row

3528

APPENDIX B

CONVERSION OF BLADE-INLET AND -OUTLET MEAN-CAMBER-LINE ANGLES

FROM A STREAM SURFACE TO A CYLINDRICAL SURFACE

For compressor designs in which the air flow is assumed to occur along stream surfaces of revolution and the blade sections are assumed to lie on the stream surfaces, some procedure for specifying constant-radius blade sections is required in order to facilitate fabrication of the blades. The method described herein provides a means for converting blade mean-camber-line angles at the inlet and outlet of a blade from a stream surface to a cylindrical surface.

Figure 12 shows the mean surface of a compressor blade - a surface described by the mean camber lines of the blade sections. Line $\overline{OA}$ (fig. 12) represents the intersection of the blade mean surface with a stream surface of revolution and is a mean camber line of a section that lies on the stream surface. Line $\overline{OB}$ represents the intersection of the blade mean surface and a cylindrical surface.

Figure 12 also shows an enlargement of that portion of the blade on the leading edge in the vicinity of the point O. This region is considered sufficiently small that all curved surfaces are assumed to be planes and all lines are assumed to be straight lines. Then straight lines $\overline{Oa}$ and $\overline{Ob}$ are portions of lines $\overline{OA}$ and $\overline{OB}$, respectively. Furthermore, the plane defined by points O, a, and e is a part of the stream surface of revolution, and the plane defined by points O, b, c, and d is a section of the cylindrical surface. The blade mean surface is also assumed to be a plane in the enlargement in figure 12. The preceding assumptions, which are intended to clarify the explanation, do not impair the rigor of the method, because the resulting equation could be obtained by considering tangent planes and tangent lines at point O.

The angle γ^o (fig. 12) is the blade mean-camber-line direction at the inlet of the blade as determined from the design relative air direction and the design value of incidence angle. This angle is measured on the stream surface. It is necessary to solve for the angle γ_*^o, which is the direction of the blade mean camber line on a cylindrical surface. The solution is derived from figure 12 as follows:

$$\tan \gamma_*^o = \frac{\overline{bc} + \overline{cd}}{\overline{Od}}$$

$$\tan \gamma^O = \frac{\overline{ae}}{\overline{Oe}} = \frac{\overline{cd}}{\overline{Oe}}$$

$$\frac{\tan \gamma^O_*}{\tan \gamma^O} = \left(\frac{\overline{bc}}{\overline{cd}} + 1\right) \frac{\overline{Oe}}{\overline{Od}} \tag{B1}$$

$$\cos \varepsilon = \frac{\overline{Od}}{\overline{Oe}} \tag{B2}$$

where ε is the angle between the compressor axis and a streamline in the $r\mathbf{z}$-plane (fig. 13(b)). (Rotation of this streamline about the compressor axis generates the stream surface of revolution.) From figure 12, it can be seen that

$$\frac{\overline{bc}}{\overline{cd}} = \frac{\overline{ed}}{\overline{Oe}} \frac{\tan \psi}{\tan \gamma^O} = \sin \varepsilon \frac{\tan \psi}{\tan \gamma^O} \tag{B3}$$

Then, substituting equations (B2) and (B3) into (B1) gives

$$\tan \gamma^O_* = \tan \varepsilon \tan \psi + \frac{\tan \gamma^O}{\cos \varepsilon} \tag{B4}$$

The problem then is the evaluation of the angle ψ, which is related to the sweep of the leading edge as follows:

$$\tan \psi = \frac{\overline{fg} + \overline{gh}}{\overline{Oh}}$$

$$\tan \psi = \tan L \tan \gamma^O_* + \tan M \tag{B5}$$

Substitution of equation (B5) into (B4) yields the following:

$$\tan \gamma^O_* = \frac{\tan \varepsilon \tan M + \dfrac{\tan \gamma^O}{\cos \varepsilon}}{1 - \tan L \tan \varepsilon} \tag{B6}$$

The same equation can be derived for a point on the trailing edge.

Figure 13 further defines the leading-edge (and trailing-edge) sweep angles and indicates the sign convention to be used in equation (B6) for both the leading and trailing edges of a blade. Angle M is positive when measured in the direction of rotor rotation from a radial line. Angle L is positive when measured in the direction of the air flow from a radial line. Angle ε is positive when the radius of the streamline increases in the direction of air flow.

The angle ε is determined from the assumed streamlines, and the angles L and M can be measured with sufficient accuracy from approximations of the $r\theta$- and rz-projections of the blade.

REFERENCES

1. Lieblein, Seymour, Lewis, George W., Jr., and Sandercock, Donald M.: Experimental Investigation of an Axial-Flow Compressor Inlet Stage Operating at Transonic Relative Inlet Mach Numbers. I - Over-All Performance of Stage with Transonic Rotor and Subsonic Stators up to Rotor Relative Inlet Mach Number of 1.1. NACA RM E52A24, 1952.

2. Lewis, George W., Jr., Schwenk, Francis C., and Serovy, George K.: Experimental Investigation of a Transonic Axial-Flow-Compressor Rotor with Double-Circular-Arc Airfoil Blade Sections. I - Design, Over-All Performance and Stall Characteristics. NACA RM E53L21a, 1954.

3. Serovy, George K., Robbins, William H., and Glaser, Frederick W.: Experimental Investigation of a 0.4 Hub-Tip Diameter Ratio Axial-Flow Compressor Inlet Stage at Transonic Inlet Relative Mach Numbers. I - Rotor Design and Over-All Performance at Tip Speeds from 60 to 100 Percent of Design. NACA RM E53I11, 1953.

4. Geye, Richard P., Budinger, Ray E., and Voit, Charles H.: Investigation of a High-Pressure-Ratio Eight-Stage Axial-Flow Research Compressor with Two Transonic Inlet Stages. II - Preliminary Analyses of Over-All Performance. NACA RM E53J06, 1953.

5. Kovach, Karl, and Sandercock, Donald M.: Experimental Investigation of a Five-Stage Axial-Flow Research Compressor with Transonic Rotors in All Stages. II - Compressor Over-All Performance. NACA RM E54G01, 1954.

6. Lieblein, Seymour, Schwenk, Francis C., and Broderick, Robert L.: Diffusion Factor for Estimating Losses and Limiting Blade Loadings in Axial-Flow-Compressor Blade Elements. NACA RM E53D01, 1953.

7. Schwenk, Francis C., Lieblein, Seymour, and Lewis, George W., Jr.: Experimental Investigation of an Axial-Flow Compressor Inlet Stage Operating at Transonic Relative Inlet Mach Numbers. III - Blade-Row Performance of Stage with Transonic Rotor and Subsonic Stator at Corrected Tip Speeds of 800 and 1000 Feet Per Second. NACA RM E53G17, 1953.

8. Carter, A. D. S.: The Low Speed Performance of Related Aerofoils in Cascade. Rep. No. R.55, British N.G.T.E., Sept. 1949.

3528

9. Robbins, William H., and Glaser, Frederick W.: Investigation of an Axial-Flow-Compressor Rotor with Circular-Arc Blades Operating up to a Rotor-Inlet Relative Mach Number of 1.22. NACA RM E53D24, 1953.

10. Laurence, James C., and Landes, L. Gene: Auxiliary Equipment and Techniques for Adapting the Constant-Temperature Hot-Wire Anemometer to Specific Problems in Air-Flow Measurements. NACA TN 2843, 1952.

11. Huppert, Merle C.: Preliminary Investigation of Flow Fluctuations During Surge and Blade Row Stall in Axial-Flow Compressors. NACA RM E52E28, 1952.

12. Timoshenko, S.: Vibration Problems in Engineering. Second ed., D. Van Nostrand Co., Inc., 1937.

3528

TABLE I. - DESIGN DATA

[Total-pressure ratio $P_4/P_3 = 1.35$, constant over blade span.]

Stream-surface radius, in.		Inlet absolute Mach number, M_3	Inlet relative Mach number, M_3'	Inlet relative air direction, β_3'	Outlet relative air direction, β_4'	Outlet relative Mach number, M_4'	Outlet absolute Mach number, M_4	Outlet absolute air direction, β_4	Total-temperature ratio, T_4/T_3	Blade-element efficiency, η	Incidence angle, i, deg	Deviation angle, δ^o, deg
Inlet, r_3	Outlet, r_4											
9.00	9.00	0.670	1.150	54.40	48.40	0.796	0.602	28.53	1.1046	0.856	3.0	1.51
8.25	8.33	.655	1.078	52.59	44.34	.752	.614	28.75	1.0990	.904	3.5	2.12
7.50	7.67	.638	1.005	50.60	39.44	.708	.627	29.54	1.0951	.941	4.0	2.82
6.75	7.00	.620	.933	48.37	33.22	.657	.643	31.27	1.0935	.958	4.5	3.67
6.00	6.33	.600	.862	45.86	25.30	.610	.663	33.77	1.0932	.961	5.0	4.59
5.25	5.67	.576	.789	43.13	15.38	.575	.691	36.67	1.0930	.961	5.5	[a]6.67
4.50	5.00	.546	.715	40.18	3.20	.557	.729	40.14	1.0930	.961	6.0	[b]8.67

[a]1° greater than Carter's rule deviation angle.
[b]2° greater than Carter's rule deviation angle.

TABLE II. - ROTATING-STALL CHARACTERISTICS

Rotor speed, percent of design	Test point (fig. 11)	Number of rotating-stall zones, λ	Rotational speed of rotor, N, rps	Absolute rotational speed of stall zones, h, rps	Relative rotational speed of stall zones, h', rps	Ratio of relative stall speed to rotor speed, h'/N	Natural frequency of rotor blades, f, cps	Ratio of disturbance frequency to natural frequency of rotor blades, λh'/f
60	A	2	130	79	51	0.39	344	0.296
60	B	1	129	75	54	.42	342	.158
80	D	1	172	96	76	.44	390	.195
50	--	2	107	65	42	.39	322	.261
50	-	1	107	60	47	.44	322	.146
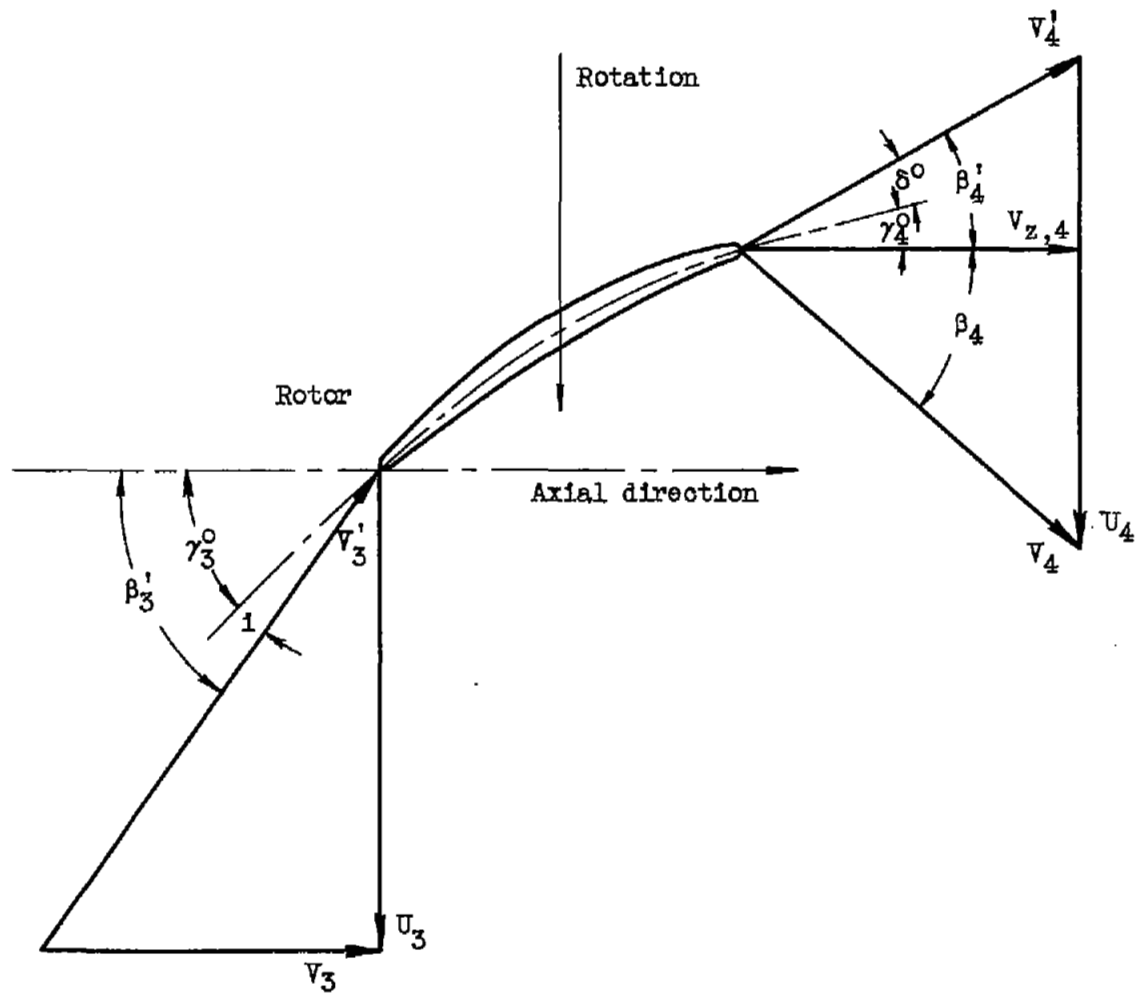
Figure 1. - Velocity-diagram notation for blade element.

3528

CY-4 back
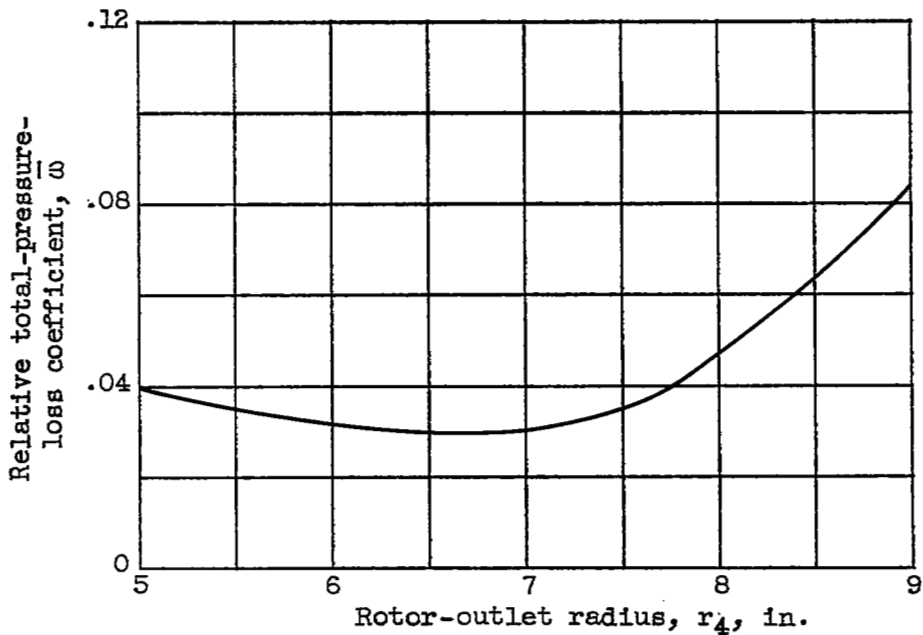
Figure 2. - Radial variation of design relative total-pressure-loss coefficient for 1.5-inch-chord transonic compressor rotor.
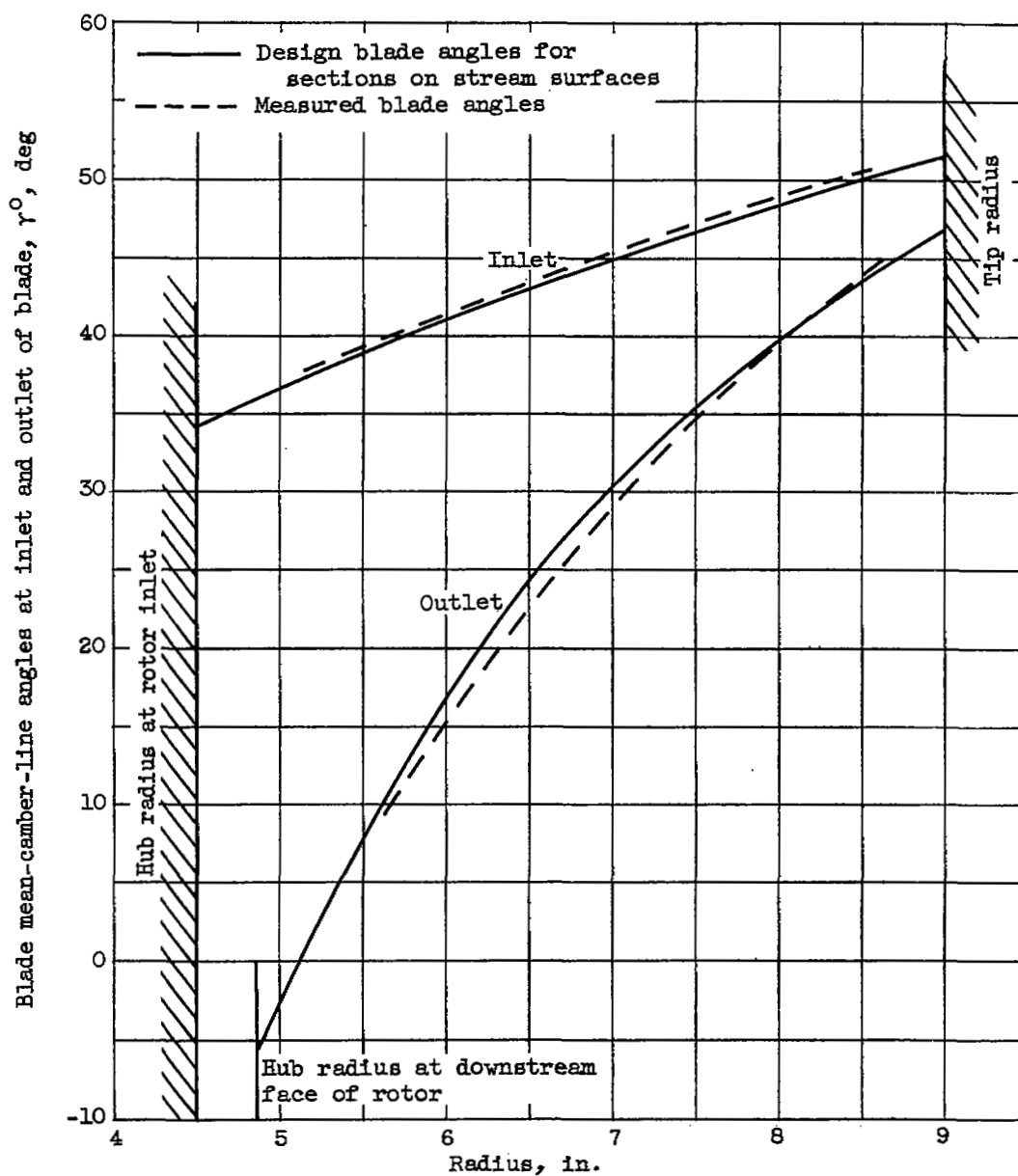
Figure 3. - Design and measured blade angles for 1.5-inch-chord transonic compressor rotor.
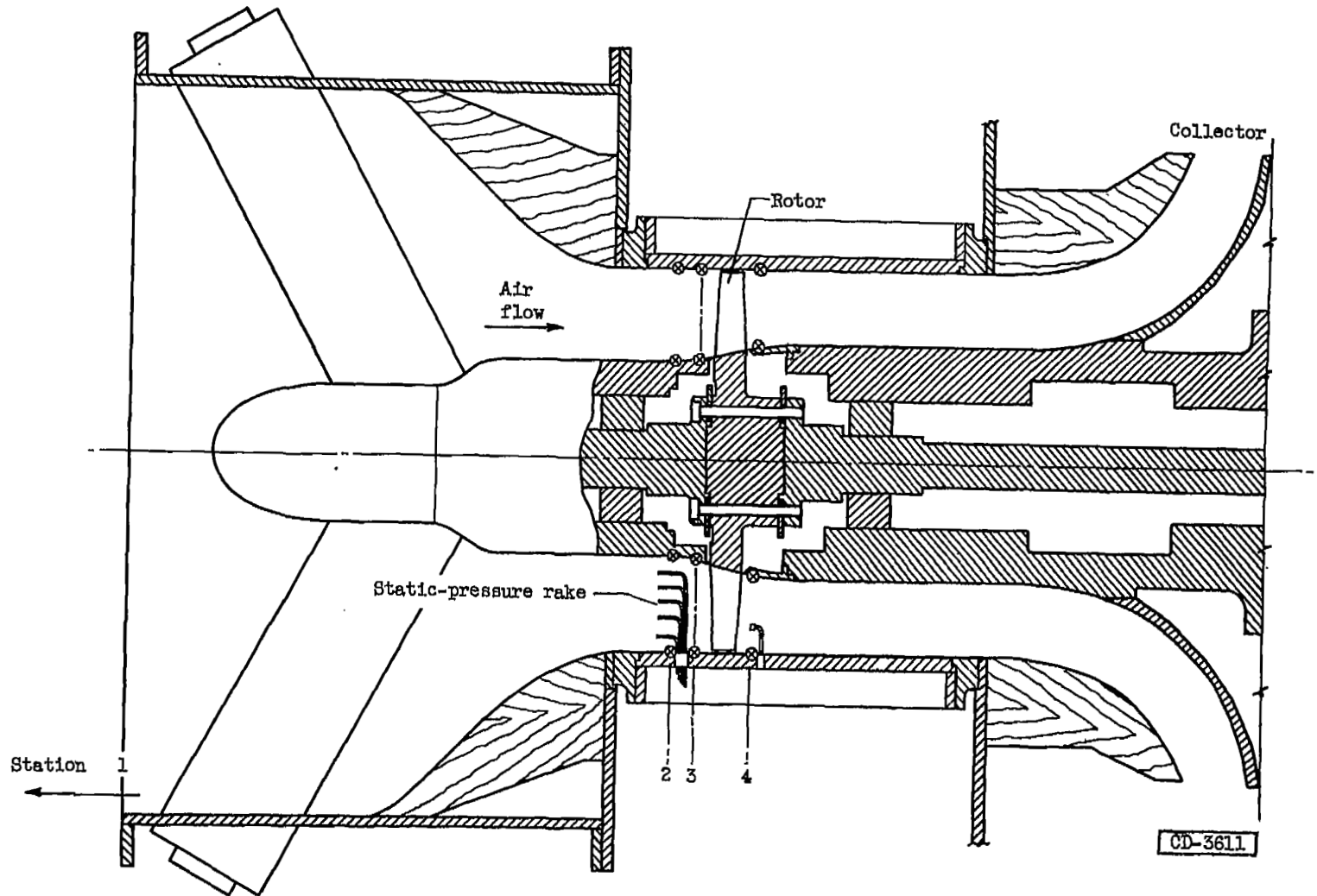
Figure 4. - Schematic diagram of transonic-compressor test rig.

3528

C-33407
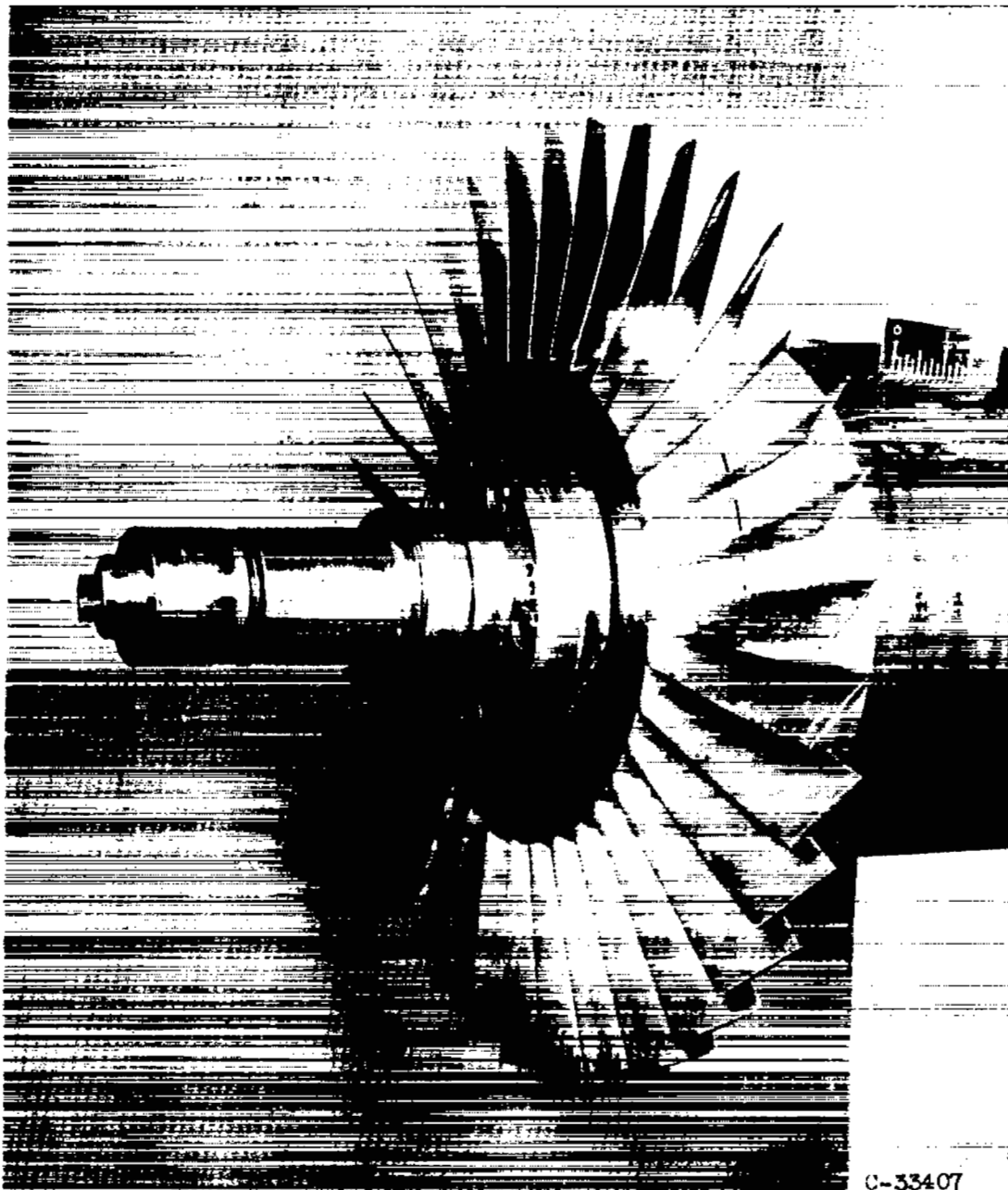
Figure 5. - 1.5-Inch-chord transonic compressor rotor.

3528

C-35353
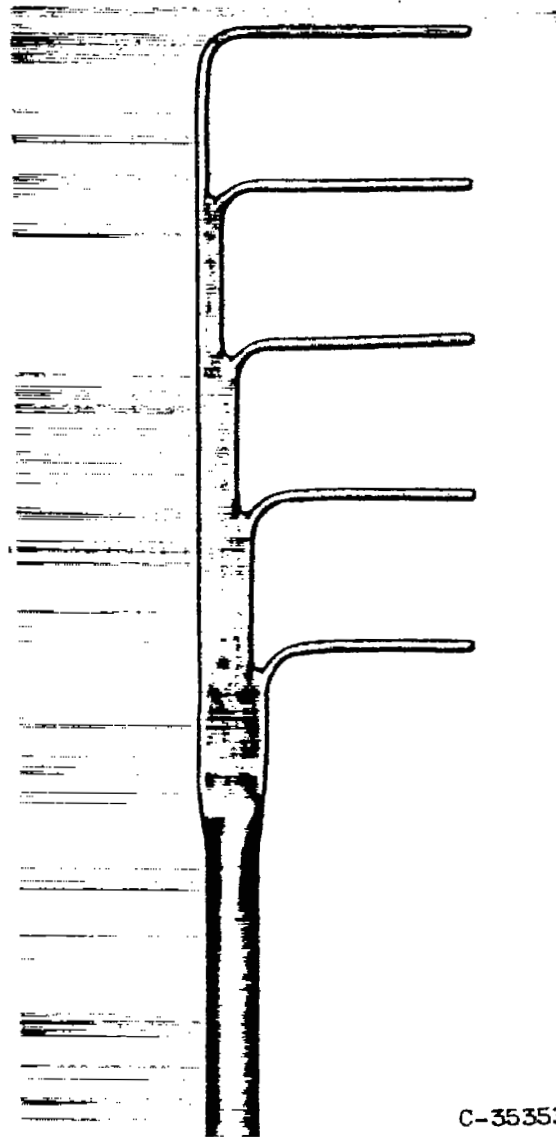
(a) Static-pressure rake.

Figure 6. - Instrumentation used in tests of 1.5-inch-chord transonic compressor rotor.
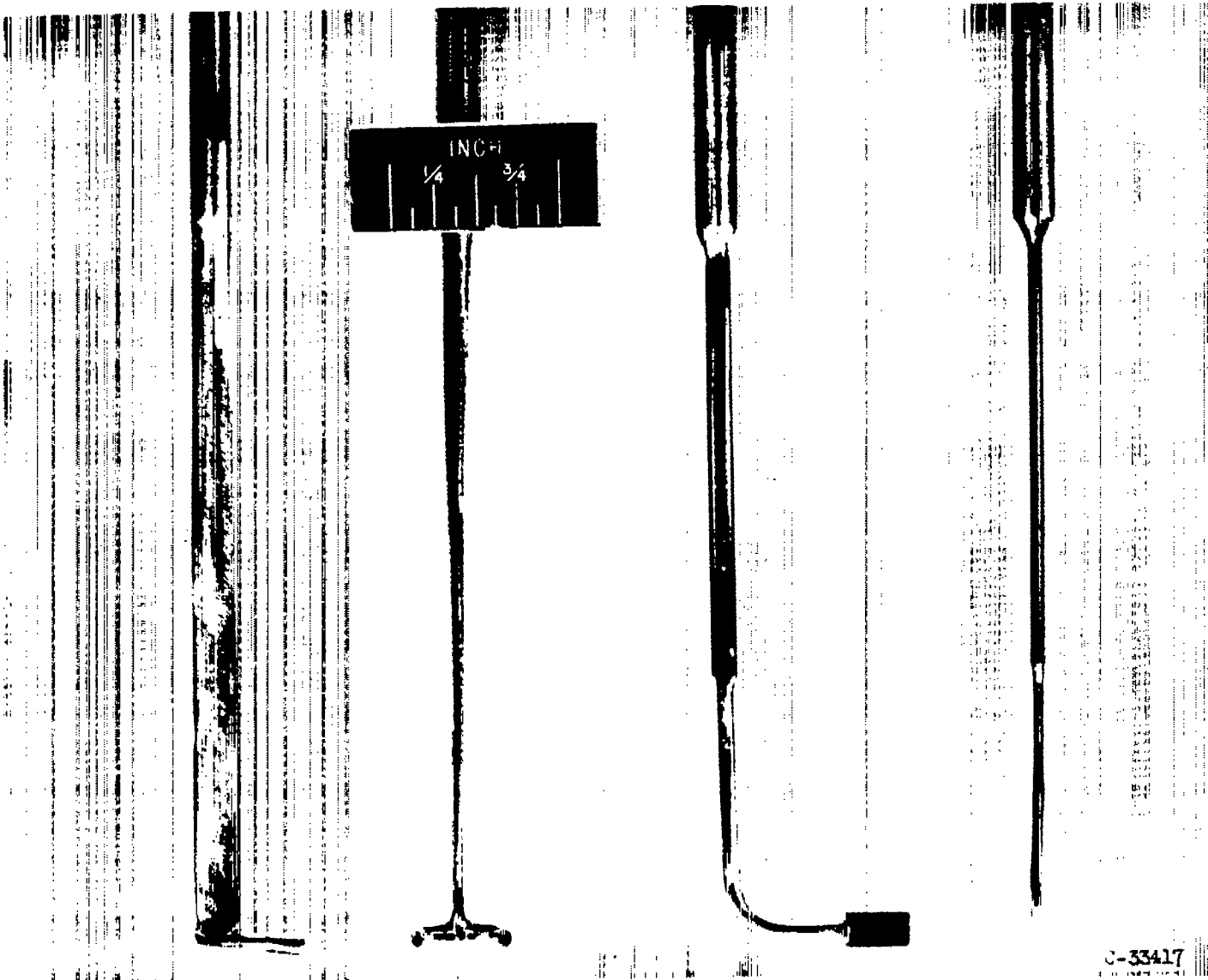
(b) Combination probe.   (c) Wedge static probe.

Figure 6. - Concluded. Instrumentation used in tests of 1.5-inch-chord transonic compressor rotor.
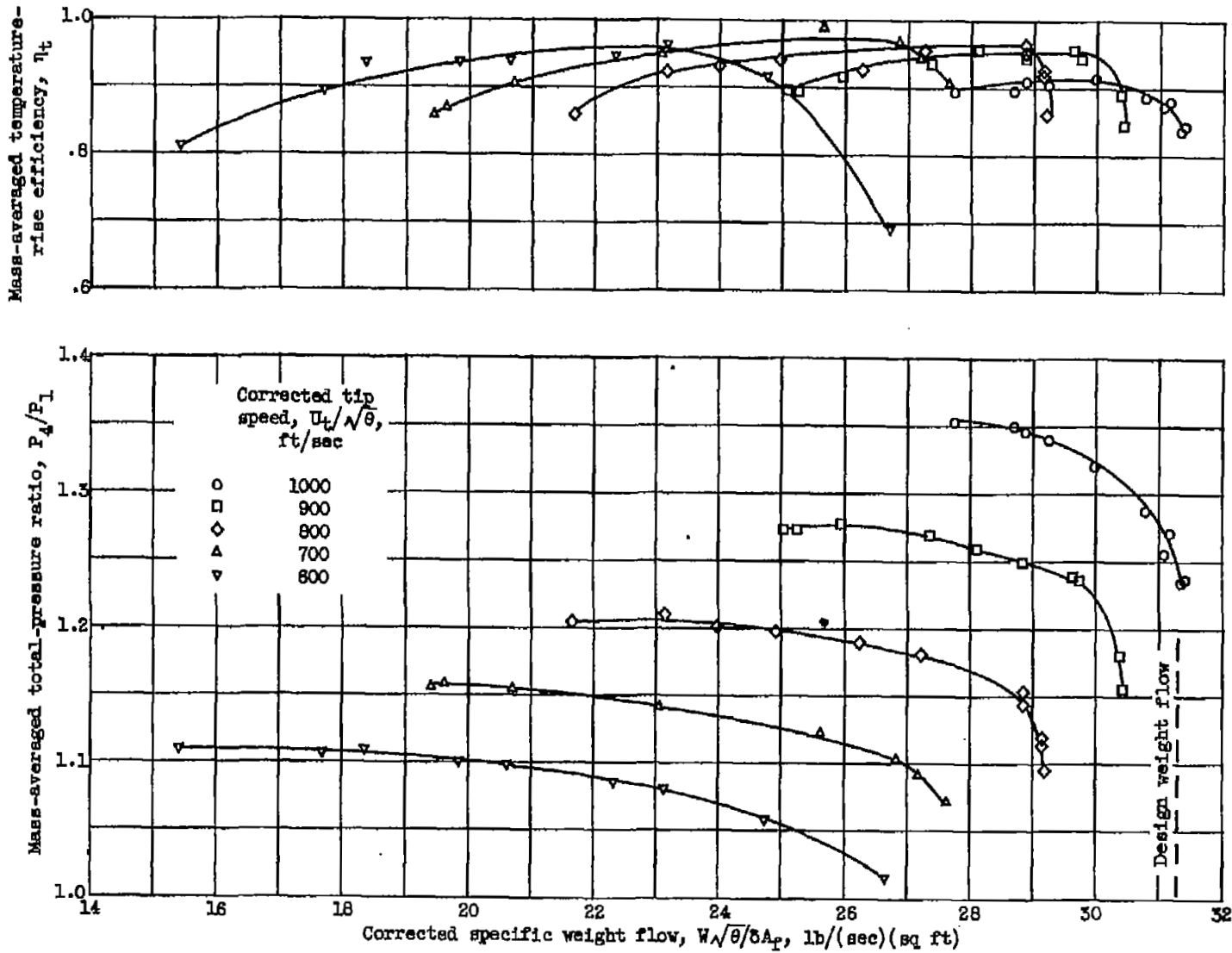
Figure 7. - Mass-averaged performance of the 1.5-inch-chord transonic compressor rotor.
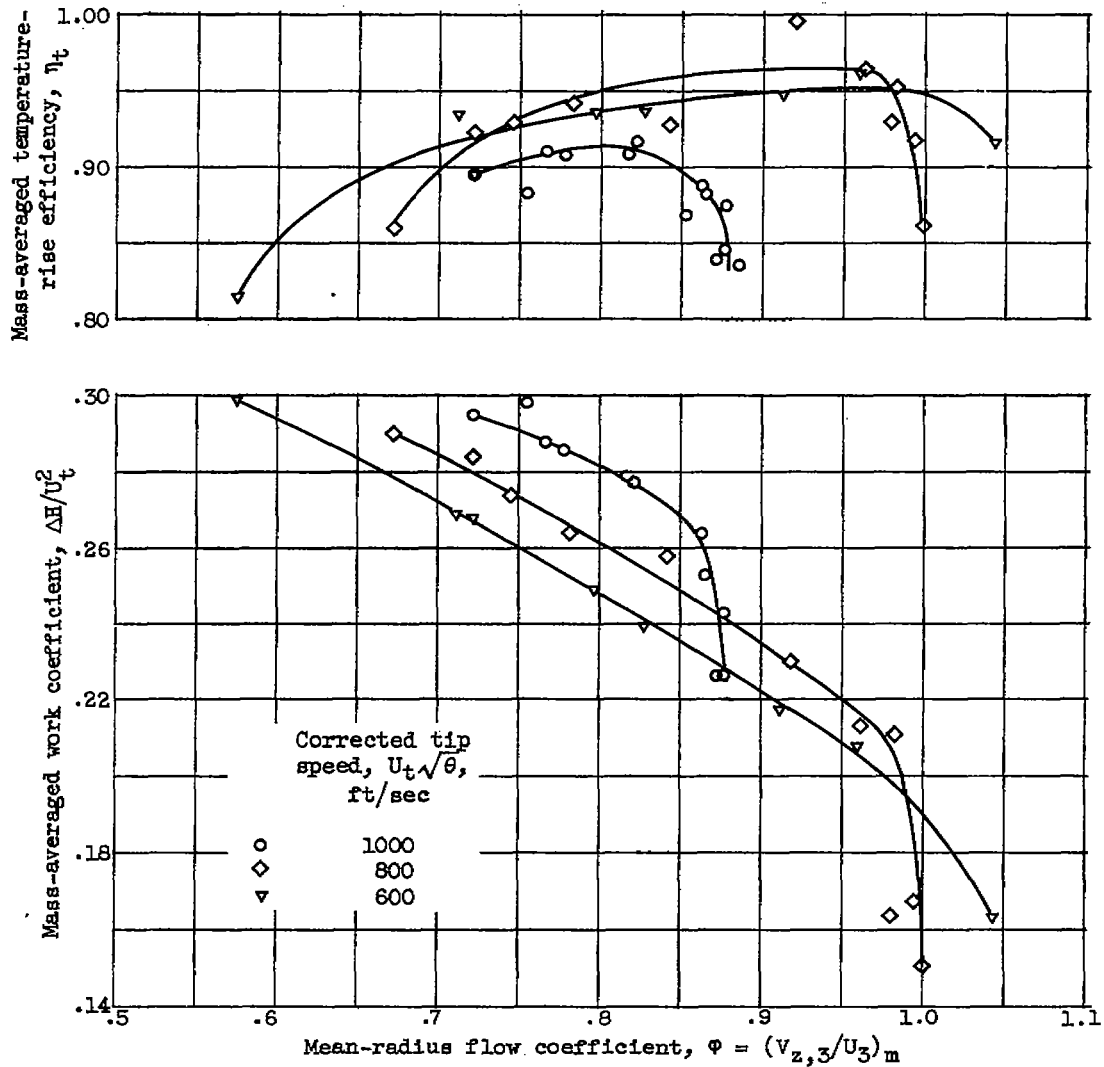
Figure 8. - Adiabatic efficiency and work coefficient against flow coefficient for 1.5-inch-chord transonic compressor rotor.
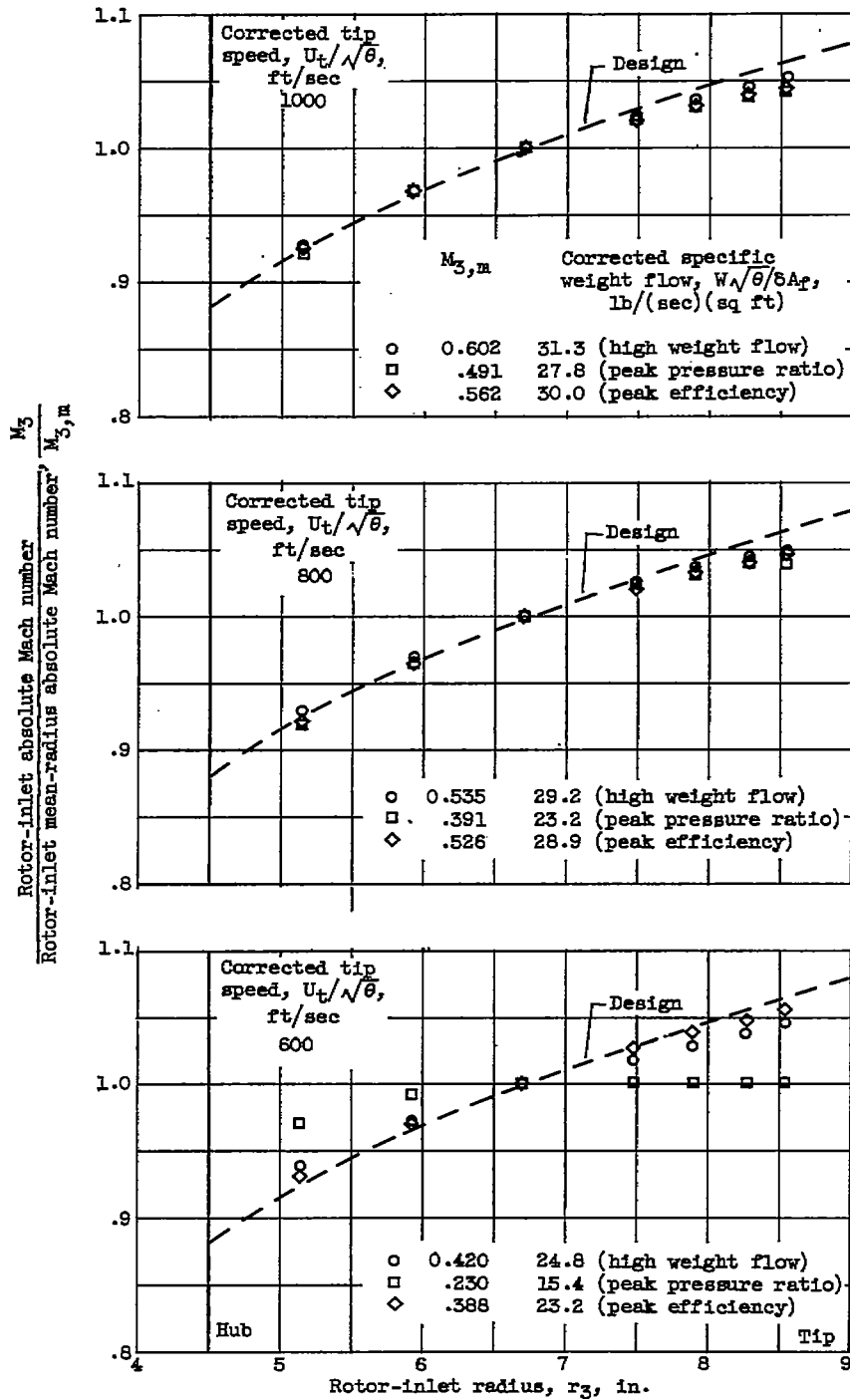
(a) Absolute Mach number.

Figure 9. - Radial variation of rotor-inlet conditions at station 3 for 1.5-inch-chord transonic compressor rotor.
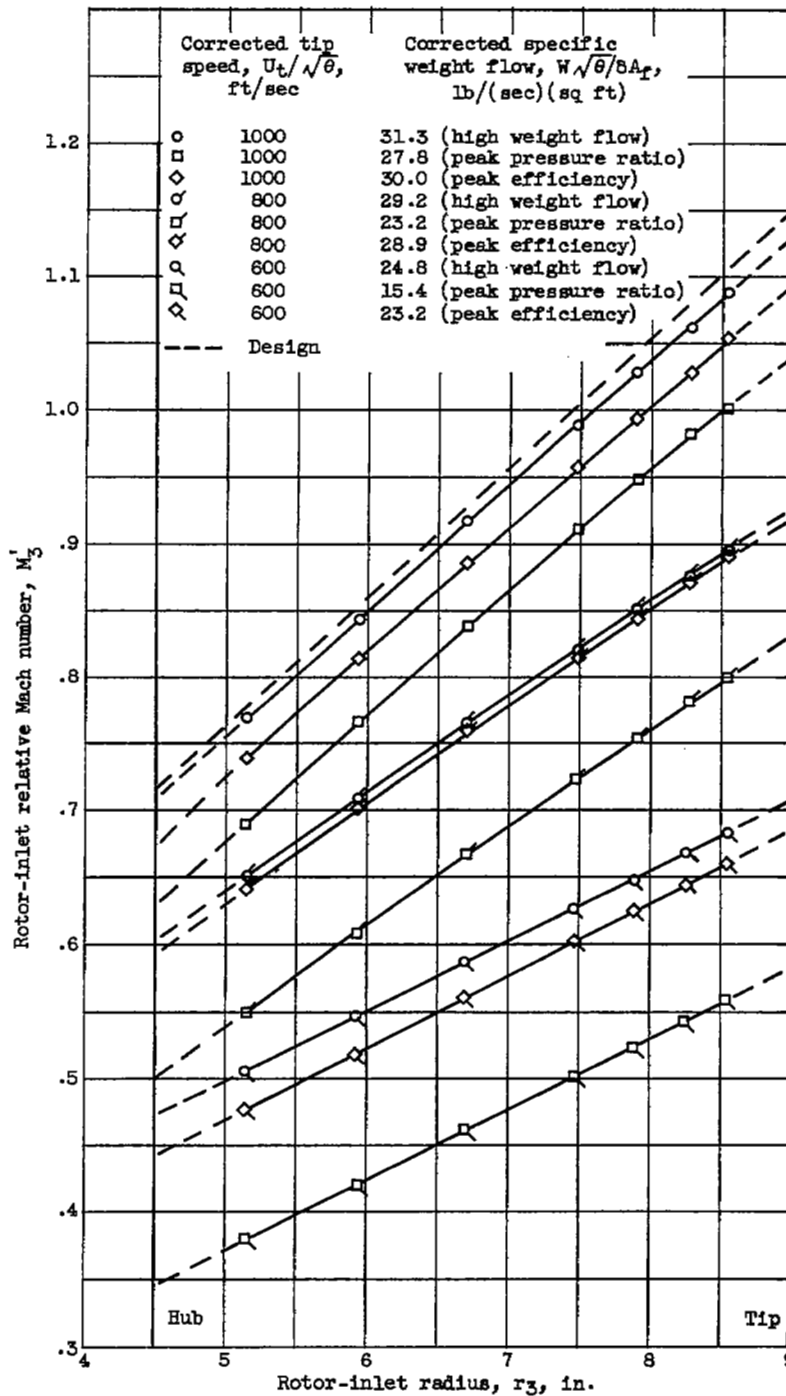
(b) Relative Mach number.

Figure 9. - Continued. Radial variation of rotor-inlet condi-
tions at station 3 for 1.5-inch-chord transonic compressor
rotor.
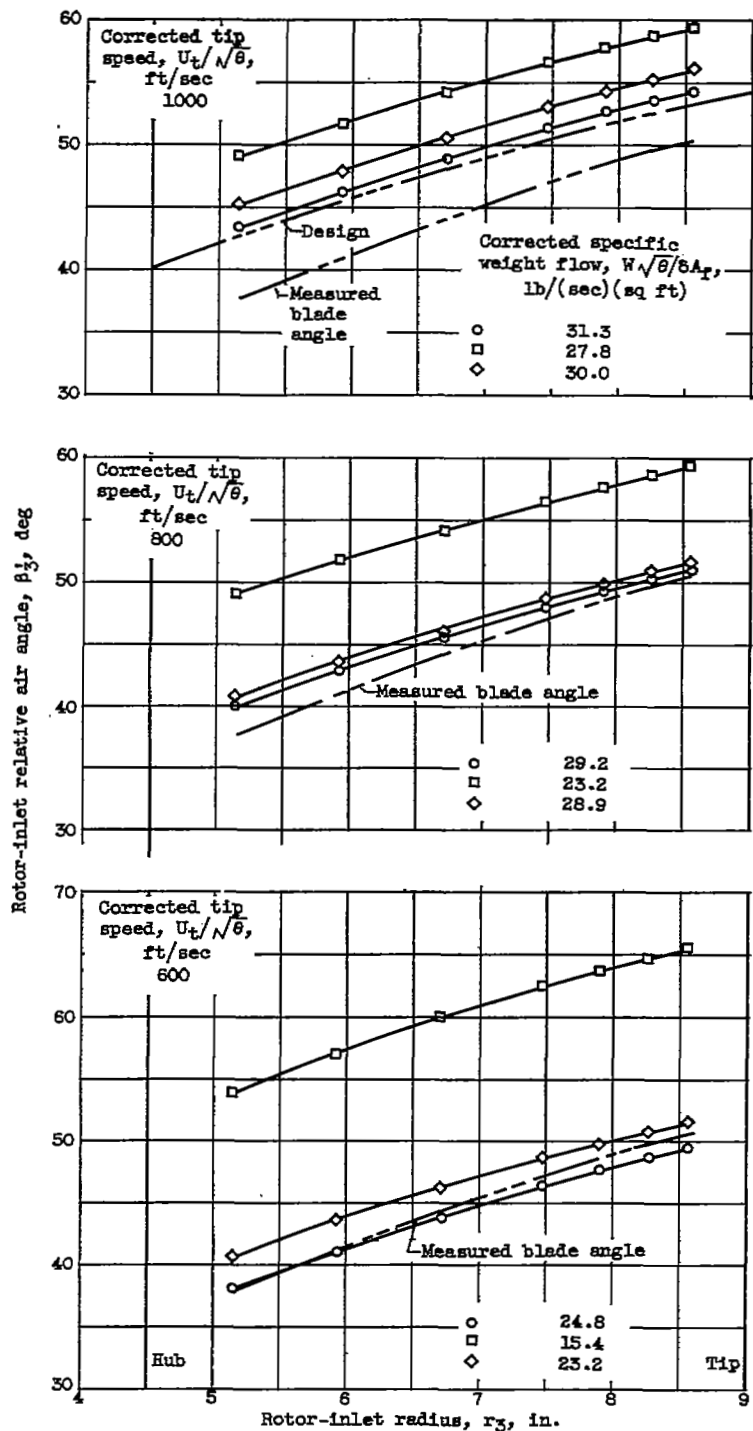
(c) Relative air angle.

Figure 9. - Concluded. Radial variation of rotor-inlet conditions for 1.5-inch-chord transonic compressor rotor.
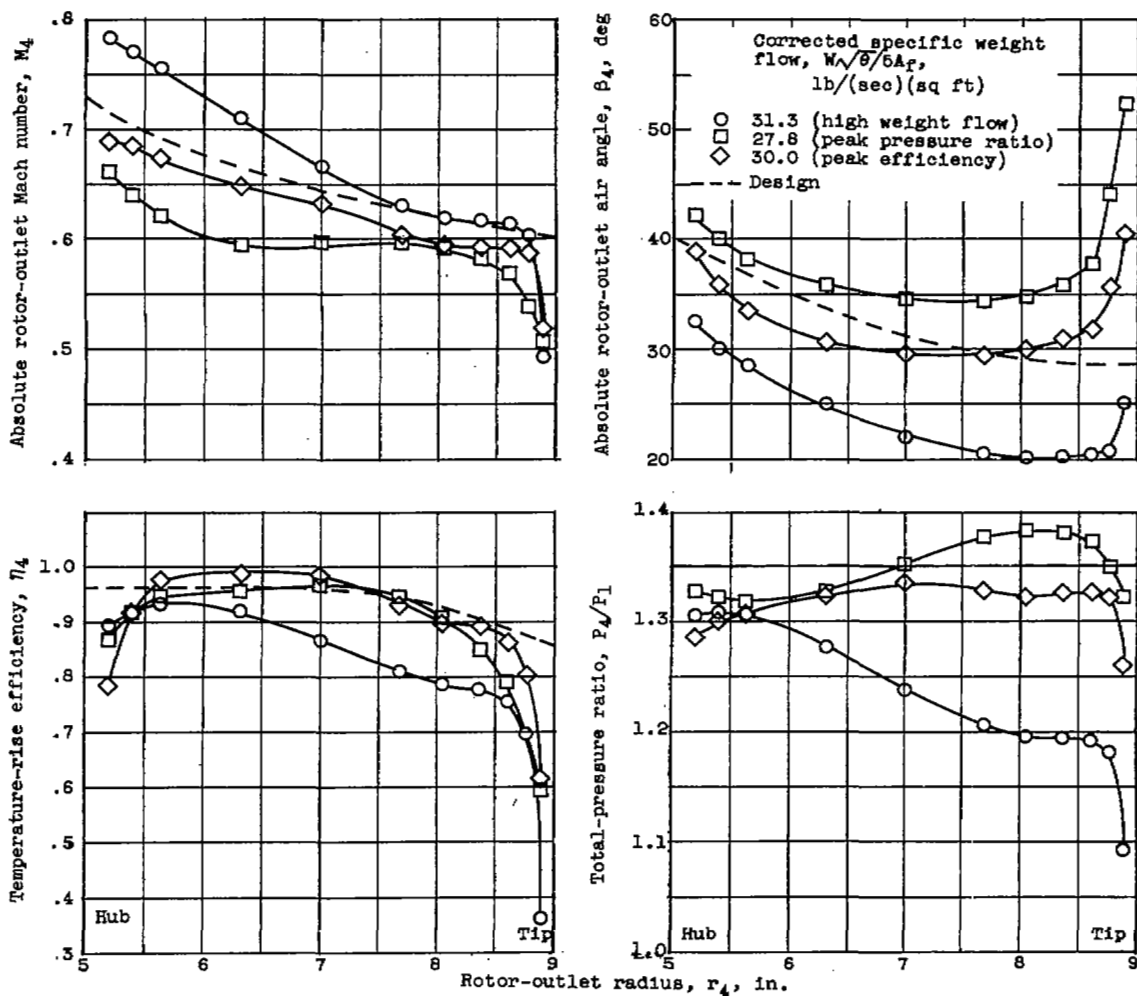
(a) Corrected tip speed, 1000 feet per second.

Figure 10. - Radial variation of rotor-outlet conditions for 1.5-inch-chord transonic compressor rotor.

3528
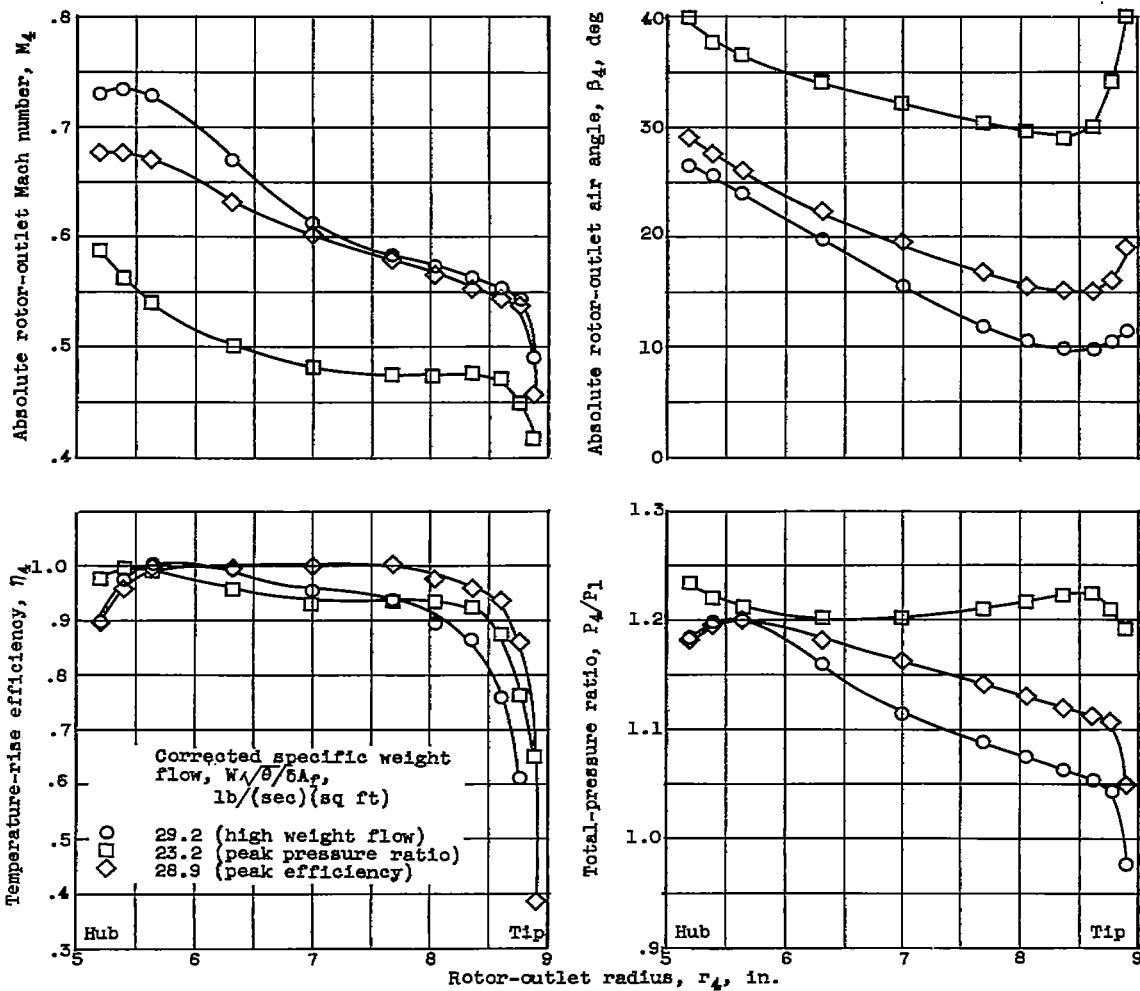
(b) Corrected tip speed, 800 feet per second.

Figure 10. - Continued. Radial variation of rotor-outlet conditions for
1.5-inch-chord transonic compressor rotor.
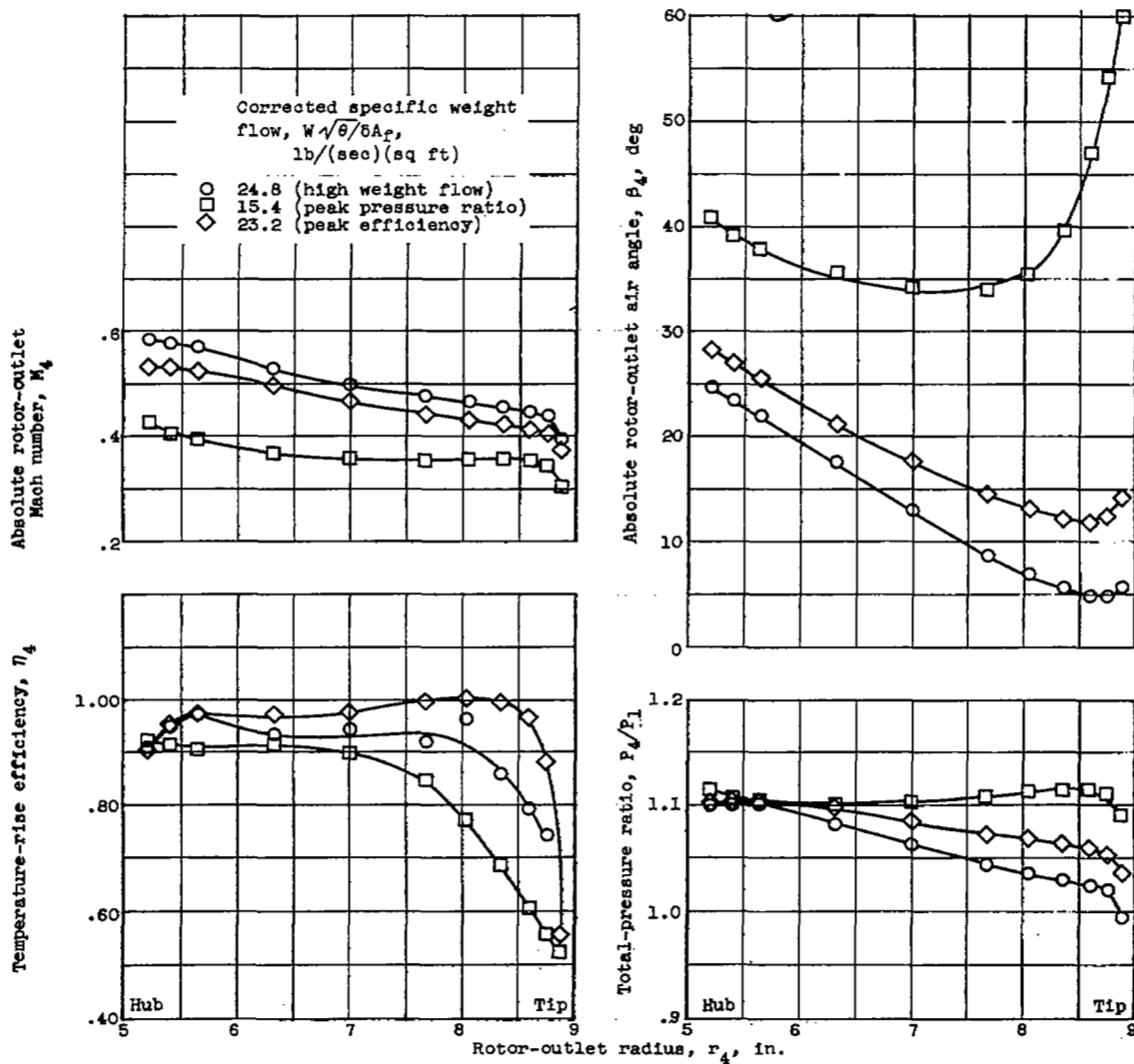
(c) Corrected tip speed, 600 feet per second.

Figure 10. - Concluded. Radial variation of rotor-outlet conditions for 1.5-inch-chord transonic compressor rotor.
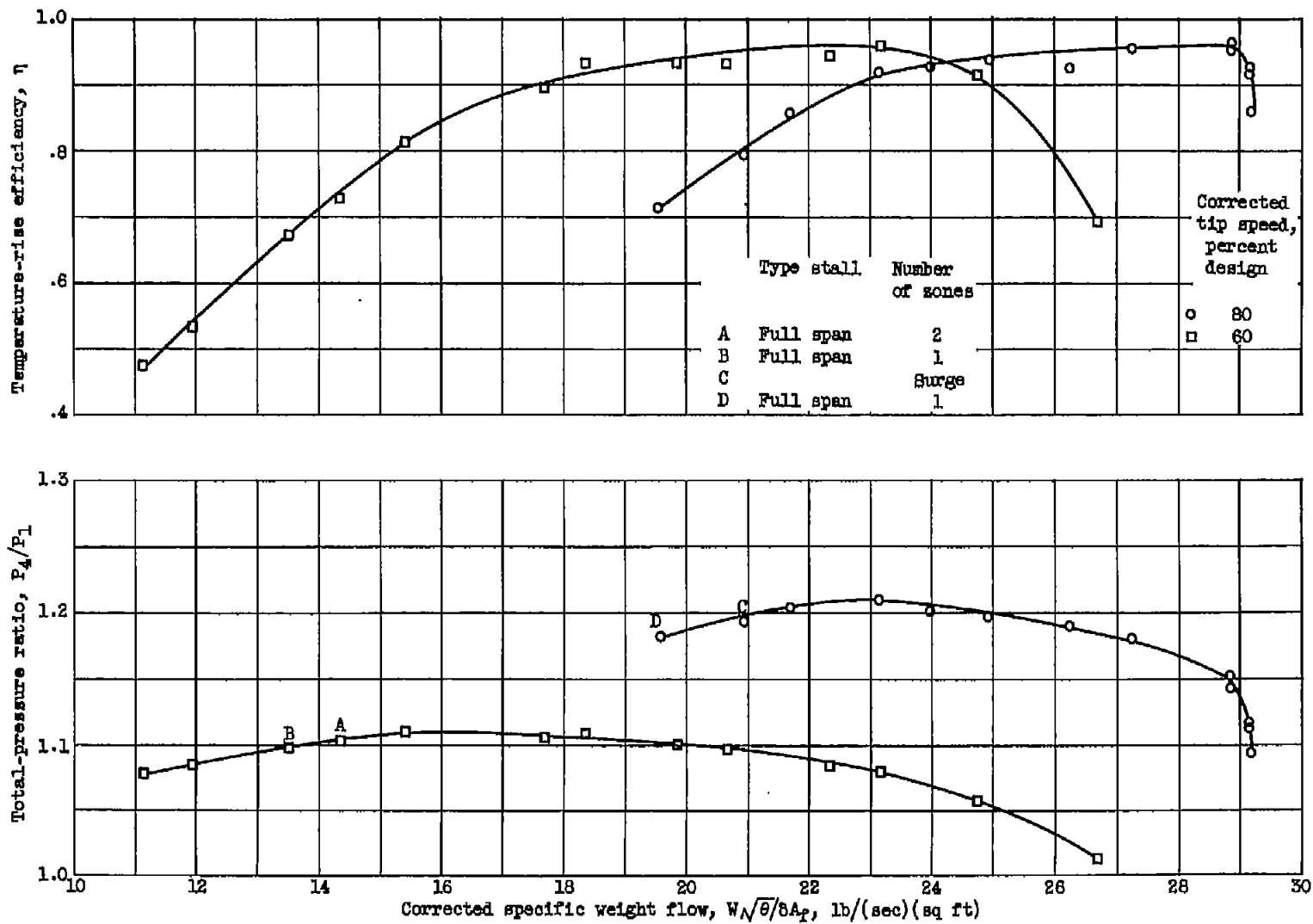
Figure 11. - Complete operating range of 1.5-inch-chord transonic compressor rotor at corrected tip speeds of 60 and 80 percent of design.
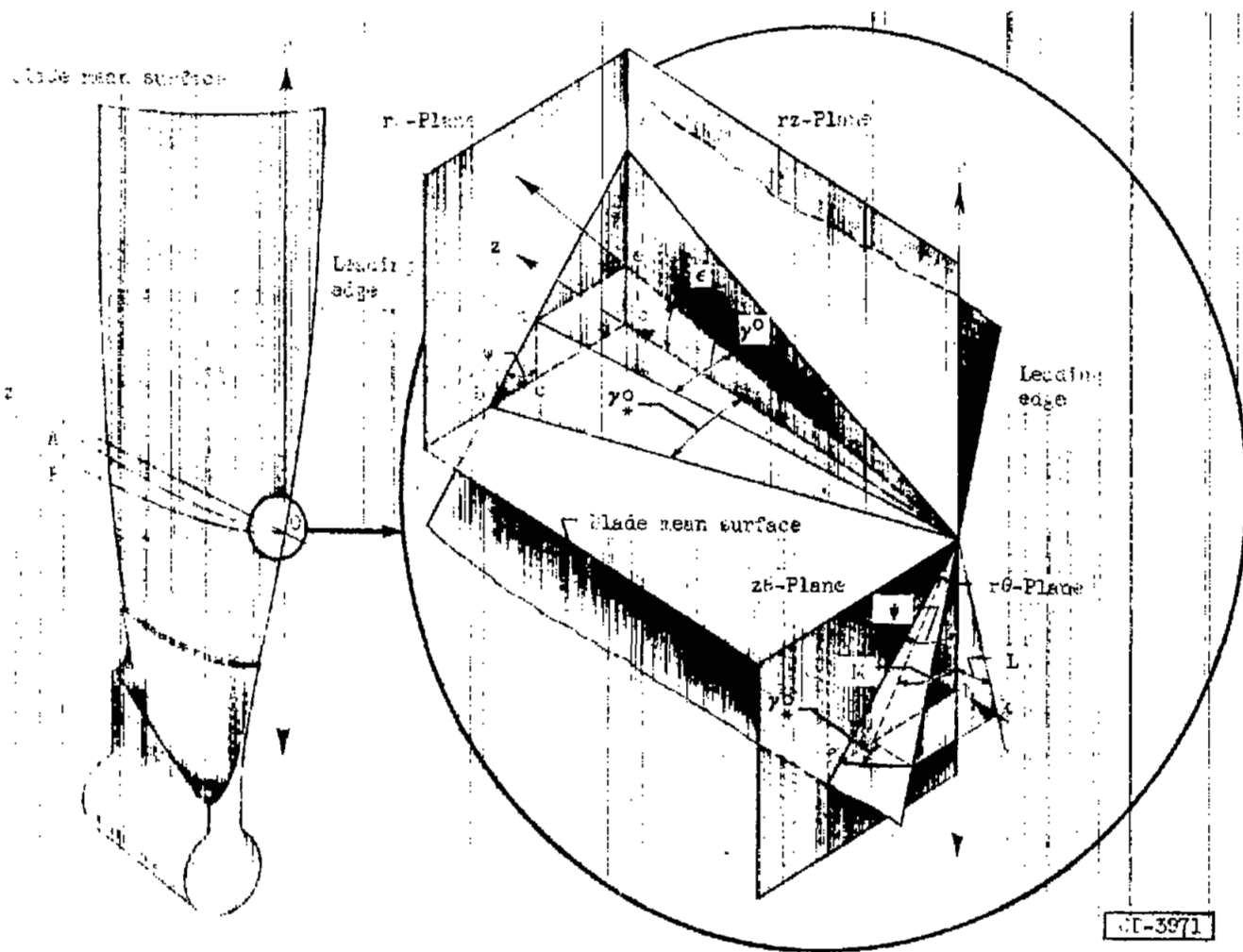
Figure 12. - Conversion of blade-inlet mean-cambar-line angles from a stream surface to a cylindrical surface.

Rotation

Trailing edge · Leading edge

-M · M

(a) rθ-Projection (front view).

Air flow

L · -L

Streamline

ε

ε

Leading edge

Trailing edge

z
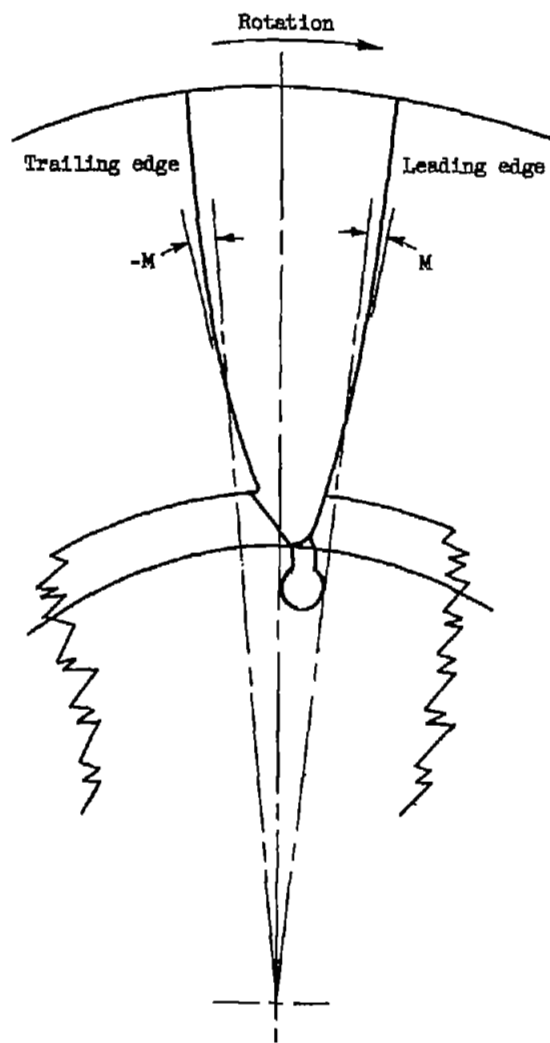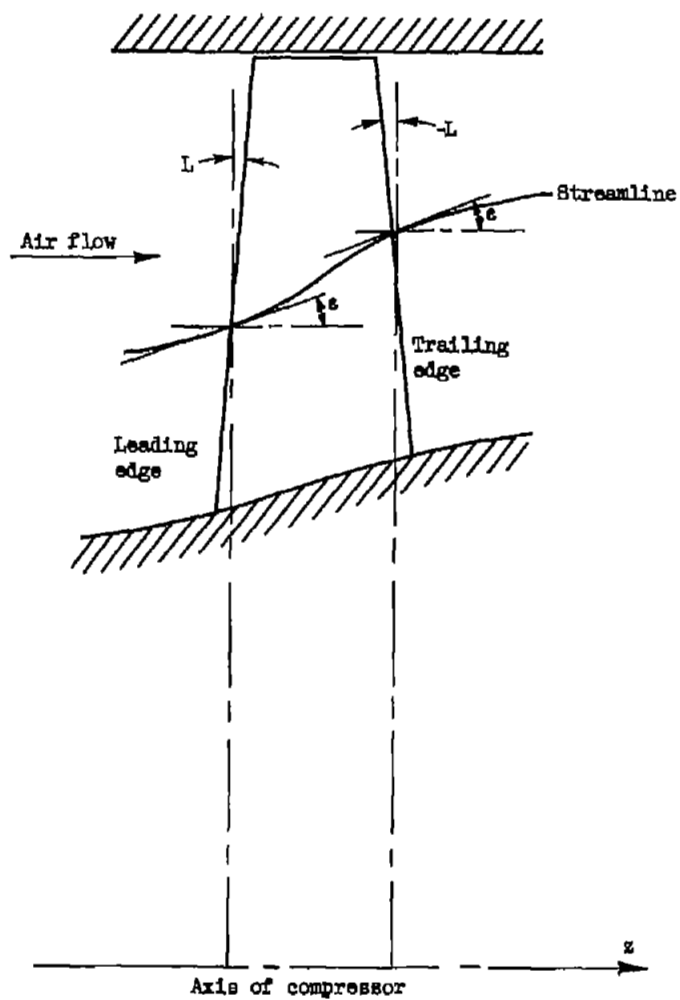
Axis of compressor

(b) rz-Projection (side view).

Figure 13. - Projections of compressor blade on rθ-plane (front view) and rz-plane (side view).